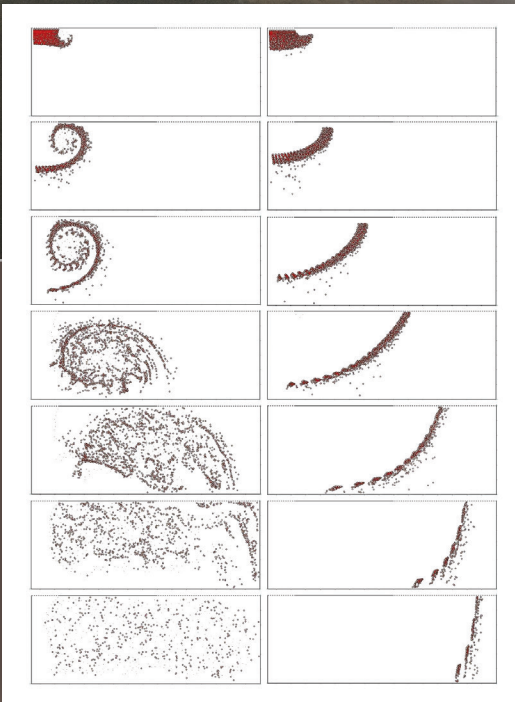
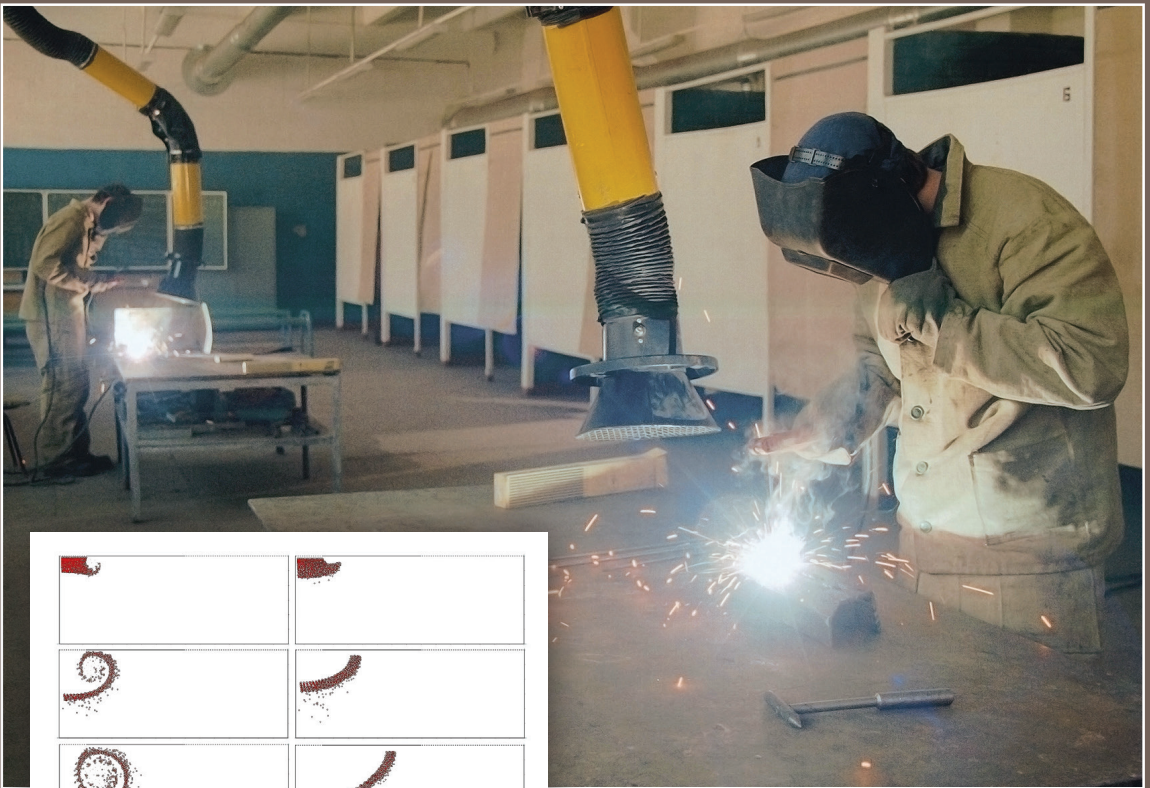


Local Exhaust Ventilation

Aerodynamic Processes and Calculations of Dust Emissions



Ivan Logachev
Konstantin Logachev
Olga Averkova

 CRC Press
Taylor & Francis Group

Local Exhaust Ventilation

**Aerodynamic Processes and
Calculations of Dust Emissions**

Local Exhaust Ventilation

Aerodynamic Processes and
Calculations of Dust Emissions

Ivan Logachev
Konstantin Logachev
Olga Averkova



CRC Press

Taylor & Francis Group

Boca Raton London New York

CRC Press is an imprint of the
Taylor & Francis Group, an **informa** business

CRC Press
Taylor & Francis Group
6000 Broken Sound Parkway NW, Suite 300
Boca Raton, FL 33487-2742

© 2016 by Taylor & Francis Group, LLC
CRC Press is an imprint of Taylor & Francis Group, an Informa business

No claim to original U.S. Government works
Version Date: 20150417

International Standard Book Number-13: 978-1-4987-2064-9 (eBook - PDF)

This book contains information obtained from authentic and highly regarded sources. Reasonable efforts have been made to publish reliable data and information, but the author and publisher cannot assume responsibility for the validity of all materials or the consequences of their use. The authors and publishers have attempted to trace the copyright holders of all material reproduced in this publication and apologize to copyright holders if permission to publish in this form has not been obtained. If any copyright material has not been acknowledged please write and let us know so we may rectify in any future reprint.

Except as permitted under U.S. Copyright Law, no part of this book may be reprinted, reproduced, transmitted, or utilized in any form by any electronic, mechanical, or other means, now known or hereafter invented, including photocopying, microfilming, and recording, or in any information storage or retrieval system, without written permission from the publishers.

For permission to photocopy or use material electronically from this work, please access www.copyright.com (<http://www.copyright.com/>) or contact the Copyright Clearance Center, Inc. (CCC), 222 Rosewood Drive, Danvers, MA 01923, 978-750-8400. CCC is a not-for-profit organization that provides licenses and registration for a variety of users. For organizations that have been granted a photocopy license by the CCC, a separate system of payment has been arranged.

Trademark Notice: Product or corporate names may be trademarks or registered trademarks, and are used only for identification and explanation without intent to infringe.

Visit the Taylor & Francis Web site at
<http://www.taylorandfrancis.com>

and the CRC Press Web site at
<http://www.crcpress.com>

Contents

Preface.....	xi
Authors.....	xiii

SECTION I Aerodynamics of Dust Airflows in the Spectra of Air Exhaust Ducts

Chapter 1	Determination of the Velocity Field by Conformal Mapping Methods.....	9
1.1	Unseparated Flows.....	9
1.1.1	General Information on the Conformal Mapping Method.....	9
1.1.2	Calculation of the Axial Air Velocity at a Freely Spaced Slot-Type Suction.....	12
1.1.3	Calculation of the Axial Air Velocity at Slot-Type Suction Built in a Flat Infinite Wall.....	14
1.1.4	Calculation of the Axial Air Velocity at a Slot-Type Suction Bell.....	16
1.2	Separated Flows.....	20
1.2.1	Calculation of the Airflow at the Slot-Type Suction Built in a Flat Infinite Wall.....	21
1.2.2	Calculation of the Airflow at the Slot-Type Suction in Infinite Space.....	24
1.3	Calculation of the Flow at the Entrance of the Slot-Type Suction Bell.....	26
1.3.1	Design Ratios.....	26
1.3.2	Calculation Results.....	34
1.4	Simulation of Flow Separation at the Inlet of a Projecting Flat Suction Channel.....	35
1.4.1	Determination of Design Ratios.....	35
1.4.2	Experimental Study.....	46
1.4.3	Calculation Results and Discussion.....	48
1.5	Mathematical Simulation of Influence of a Screen on the Aerodynamic Drag Value of a Suction Slot.....	53
1.5.1	Determination of Design Ratios.....	53
1.5.2	Calculation Results and Discussion.....	63
1.5.3	Conclusions.....	68
1.6	Simulation of Air Jet Flow at the Inlet into a Hooded Flat Channel Equipped with an Impermeable Screen.....	69
1.6.1	Construction of Design Ratios.....	69
1.6.2	Calculation Results and Discussion.....	75
1.6.3	Conclusions.....	79
1.7	Laws of Separated Flows at the Inlet into a Projecting Channel with Screens.....	79
1.7.1	Determination of Design Ratios.....	79
1.7.2	Findings of the Study.....	91

Chapter 2	Calculation of Flat Potential Flows by the Boundary Integral Equation Method ...	101
2.1	Flow Superposition Method	101
2.1.1	Line and Point Sinks	101
2.1.2	Simplest Examples of the Application of Flow Superposition Method	103
2.1.3	Calculation of the Axial Air Velocity at Suction Inlets Built in a Flat Wall	106
2.1.4	Screening of a Local Suction by Supply Air Jets.....	111
2.2	Boundary Integral Equations Method.....	118
2.2.1	Flat Flows in Multiply-Connected Regions without Singularities... 118	
2.2.1.1	Derivation of the Basic Relations and the Construction of Stages of Solution	118
2.2.1.2	Discretization of the Area Boundary.....	121
2.2.1.3	Calculation of the Strength of Sources (Sinks).....	121
2.2.1.4	Calculation of the Air Velocity inside the Flow Area	126
2.2.1.5	Test Problem: Calculation of the Axial Air Velocity at Slot-Type Suction Units	126
2.2.1.6	Dedusting the Casting Roller Processing Procedure.....	127
2.2.2	Flat Flows in Multiply-Connected Regions with Cuts.....	134
2.2.3	Flat Flows in Multiply-Connected Regions with Rotating Cylinders	141
2.2.4	Three-Dimensional Flows in Multiply Connected Regions without Singularities	145
2.2.4.1	Derivation of the Basic Relations and the Construction of Main Stages of Solution	145
2.2.4.2	Discretization of the Boundary Surface Local Coordinates.....	147
2.2.4.3	Determination of the Boundary Strengths of Sources and Sinks	150
2.2.4.4	Test Problem: Calculation of the Axial Air Velocity at Rectangular Suction Inlet Built in a Flat Infinite Wall	154
2.2.4.5	Calculation of the Air Flow Sucked by a Rectangular Suction That Flows around a Cylinder (Suction from a Roll-Turning Machine).....	155
2.2.4.6	Determination of the Optimal Geometric Parameters of Local Suction Units of Automatic Presses	160
2.2.5	Three-Dimensional Flows in Multiply Connected Regions with Rotating Cylinders	162
Chapter 3	Calculation of Vortex Flows.....	167
3.1	Frictional Flows.....	167
3.1.1	Basic Equations: General Algorithm of Numerical Calculation.....	167
3.1.2	Flow Area Discretization Discrete Countertypes of Integral Equations	168
3.1.3	Calculating F and G Matrix Elements	172
3.1.4	Calculating L and H Matrix Elements	175
3.1.5	Test Case: Backward Step Flow	179
3.1.6	Calculation of the Mutual Effect of Two Straight Supply Air Jets	180
3.2	Flow Simulation Using a Vortex Layer	184

- 3.3 Vortex Flow around a Slot-Type Suction above the Right Dihedral Angle..... 189
 - 3.3.1 Numerical Computation Algorithm 189
 - 3.3.2 Calculation Data 193
- 3.4 Nonstationary Flows around Slot-Type and Round Suction Units 196
 - 3.4.1 Flow around a Slot-Type Suction Unit in an Unlimited Space 196
 - 3.4.2 Flows around Slot-Type Bell-Shaped Suction Units 203
 - 3.4.3 Round Bell-Shaped Suction Units..... 209
 - 3.4.4 Experimental Determination of Local Drag Factors of Profiled Local Exhausts 212
- 3.5 Supply Air Jet Suction United Exhausts..... 218
- 3.6 Closed Region Flows: Model Problems 223
 - 3.6.1 Approach Flow past a Thin Suction Unit 223
 - 3.6.2 Approach Flow past a Rectangular Offset 223
 - 3.6.3 Two-Dimensional Turbulent Jet Flowing out of a Plane Wall Slot 224
 - 3.6.4 Circulation Flows in a Rectangular Region 225
 - 3.6.5 Airflow Dynamics in a Room with an Offset 228
- 3.7 Modeling Flows in Thin Screen Areas (Slot-Type)..... 233
 - 3.7.1 Problem Setup 233
 - 3.7.2 Deriving the Basic Design Relations..... 234
 - 3.7.3 Modeling Vortex Flows in a Slot-Type Suction Unit Equipped with Mechanical Screens 237
 - 3.7.4 Modeling Vortex Flows in a Trapezoidal Area..... 243
- 3.8 Modeling Separated Flows Using Stationary Discrete Vortices 249
 - 3.8.1 Flow Separation Upstream of a Two-Dimensional Protruding Suction Duct 249
 - 3.8.1.1 Basic Design Relations and Computation Algorithm..... 249
 - 3.8.1.2 Calculation Data and Its Discussion 254
 - 3.8.2 Flow Separation Upstream of a Two-Dimensional Suction Duct, Covering a Thin Profile with a Noncirculatory Flow past It 257
 - 3.8.2.1 Deriving Basic Design Relations 257
 - 3.8.2.2 Analysis of a Separated Flow Upstream of a Two-Dimensional Duct with Two Screens 259
 - 3.8.3 Regarding Circulatory and Shock-Free Flow around Profiles within the Range of a Two-Dimensional Suction Duct..... 262
 - 3.8.3.1 Computational Approach Description 262
 - 3.8.3.2 Full-Scale Experiment Arrangement Description 266
 - 3.8.3.3 Analysis of a Separated Flow Upstream of a Protruded Duct with a Vertical Profile 267
 - 3.8.4 Separated Flow around Profiles within the Range of a Suction Duct 272
 - 3.8.4.1 Computation Algorithm..... 272
 - 3.8.4.2 Calculation Data and Its Discussion 276

Chapter 4 Behavior of Dust Particles in the Suction Range 279

- 4.1 Modeling the Behavior of Single Dust Particles in the Range of Semiclosed and Closed Exhaust Ducts 279
 - 4.1.1 Calculating the Required Volumes of Suction in Self-Cleaning and Overhead Drilling..... 279
 - 4.1.2 Computation of Dust Particle Paths in Silo Bin Cavities 283

4.1.3	Forecasting Particle Size Distribution and Concentration of Coarsely Dispersed Aerosols	287
4.2	Analysis of Dust Particle Dynamics Induced at Open Local Exhausts by Rotating Cylinders.....	300
4.3	Modeling Dust Particle Dynamics in Suction Units with Rotating Cylinders	304
4.3.1	Model Problems	306
4.3.2	Calculating the Maximum Diameter of Dust Particles from Single-Wall Hoods.....	307
4.3.3	Calculating the Maximum Diameter of Dust Particles from Double-Wall Hoods	308
4.3.4	Calculating the Maximum Diameter of Dust Particles from Double-Wall Hoods Equipped with a Rotating Cylinder.....	310
4.3.5	Calculating the Maximum Diameter of Dust Particles from Double-Wall Hoods Equipped with Two Rotating Cylinders	315
4.3.6	Calculating the Maximum Diameter of Dust Particles from Double-Wall Hoods Equipped with a Rotating Cylinder and a Suction Cylinder.....	316
4.4	Modeling the Behavior of Dust Particles in Pulsating Flows	316
4.4.1	Deriving Basic Design Relations.....	317
4.4.2	Calculation Data and Discussion.....	319
4.5	Modeling the Behavior of Polyfractional Aerosol in a Suction Unit	324
4.5.1	Algorithms for Computation of Flows in Regions with Multiple Suction Cylinders	324
4.5.2	Forecasting Particle Size Distribution and Concentration of Coarsely Dispersed Aerosols in Local Exhaust Air.....	327
4.5.3	Analysis of Variation in the Particle Size Distribution and Concentration of Dust Particles in a Rotating Suction Cylinder Located in a Suction Unit.....	328
4.5.4	Dust Aerosol Behavior in a Suction Unit of Standard Configuration.....	330
4.6	Some Gas–Dust Flow Calculation Data Obtained Using RANS and LES Methods	336
4.6.1	Modeling Three-Dimensional Gas–Dust Flows	340
4.6.1.1	Parallelization of Computations	343
4.6.2	Modeling Two-Dimensional Flow in a Suction Unit with Air Inflow through Slots.....	344

SECTION II *Recirculation of Ejected Air in Chutes*

Chapter 5	Specific Features of Air Ejection in a Perforated Duct with a Bypass Chamber.....	385
5.1	One-Dimensional Dynamics Equations for Ejected and Recycled Air	385
5.2	Linearization of Relative Motion Equations for Air Ejected in a Perforated Pipe	390
5.3	Numerical Studies	393
5.3.1	Estimating Boundary Conditions.....	393
5.3.2	Special Case for Air Ejection in a Pipe with Impermeable Walls ($E = 0$).....	395

5.3.3	Averaging Functions and Simplifying Equations	401
5.3.4	Special Concerns of a Numerical Study	405
5.3.5	Linearizing the Equation for Absolute Motion of Ejected Air	408
5.3.6	Comparing Integration Results	412
5.4	Specific Behavior of Air Recirculation in a Transfer Chute with a Combined Bypass Chamber	415
5.4.1	Original Equations	415
5.4.2	Special Case with Bypassing a Nonperforated Chute	421
5.4.3	Efficiency of Combined Bypass	427
5.5	Conclusions.....	435
Chapter 6	Air Ejection in a Porous Pipe with Linear Cross-Flow Pattern	437
6.1	Porous Pipe without Bypass	438
6.1.1	One-Dimensional Flow Equations for Air Ejected in a Porous Pipe.....	438
6.1.2	Findings from Studies	442
6.2	Porous Pipe with a Bypass Chamber.....	447
6.2.1	Analytical Solutions	447
6.2.2	Numerical Examinations.....	450
6.2.3	Findings from Studies	451
6.2.3.1	Specific Features of Recirculation.....	451
6.2.3.2	Change in Ejected Air Velocity.....	457
6.2.3.3	Pressure Variations	459
6.3	Conclusions.....	464
Chapter 7	Specific Features of Air Ejection in Elevator Handling of Grain	467
7.1	Variation of Ejection Heads Created by Falling Particles in Chutes with Varying Frontal Drag Coefficients	467
7.2	Ejecting Properties of a Bucket Elevator.....	474
7.3	Cross Flow of Air through Sealed Elevator Enclosures.....	483
7.4	Conclusions.....	494
Chapter 8	Measures for Reducing Aspiration Volumes in Elevator Handling of Grain	497
8.1	Aerodynamic Performance of Elevator Buckets	497
8.2	Features of the Proposed Design for Aspiration Layout of Grain Elevators	501
8.3	Aspiration Volumes	507
8.4	Reducing Required Aspiration Volumes in Bypassed Elevator Handling Systems.....	511
8.5	Conclusions.....	529
References	533

Preface

This book expounds the theory behind design computations of gas-borne dust flows in local exhaust ventilation systems and provides practical recommendations on energy-efficient containment of gas-borne dust emissions.

The basic approaches to operational energy savings for local exhaust ventilation systems are discussed briefly, including shaping intake openings of open local exhaust devices after determining the boundaries of vortex areas, increasing the working distance of suction openings, inhibiting carryover of dust into aspiration network by promoting rotational aerodynamic fields and installing mechanical screens, minimizing air intake through leaking gaps of aspiration cowls by using mechanical screens and leveraging the jet separation effect, and promoting recirculation in aspiration cowls to suppress ejection of air.

Section I comprises a survey of separated and vortex currents in exhaust duct spectra. Topics covered include determination of vortex field boundaries, development dynamics of vortex flow patterns, and interaction between the exhaust plume and inflow jets. The behavior of individual dust particles and the polydisperse pluralities of dust particles are studied in effective spectra of exhaust ducts. Various classes of problems are considered together with open and closed configurations of local ventilated suction units.

The methods used for surveying currents in local exhaust ventilation systems include those known from the theory of the functions of a complex variable and ideal incompressible liquid jet theory, boundary integral equations method, discrete vortex methods for stationary and nonstationary problems, vortex method, and numerical method for solving Reynolds-averaged Navier–Stokes equations and continuity equations.

Section II deals with the aerodynamics of loose-matter handling in porous ducts and the identification of regularities in air circulation patterns in bypass ducts. Differential equations for air ejection by a flow of loose matter have been put forward and subsequently solved and studied to demonstrate theoretically the capability for a manifold reduction of aspiration volume by optimizing the parameters of loading facilities. The case of grain handling in bucket elevators is used to illustrate ejection effects of air cross-flow patterns both in adjacent loading and discharge chutes and in the enclosures of the carrying and return runs of a bucket elevator.

The book may be of interest to researchers in fields such as aerodynamics of dust-control ventilation, mechanics of heterogeneous media, and fluid mechanics. It may be of value for process and mechanical engineers and designers involved in ventilation systems design, as well as supervisors of dust-control and ventilation facilities at industrial plants. The book will be useful to young scientists, undergraduate and postgraduate students majoring in the design of heat/gas supply and ventilation systems, occupational safety and health, environmental safety, and fluid mechanics.

Research findings published here would not have been possible without the financial support from the Grants Council of the President of Russia (Project MK-103.2014.1), the Russian Basic Research Foundation (Project No. 14-41-08005r_ofi_m, 14-08-31069mol_a), and the Strategic Development Program of the Belgorod State Technological University (Project No. A-10/12).

Authors



Ivan Nikolayevich Logachev holds a doctorate in engineering and is professor and academician at the Russian Academy of Natural Sciences, Moscow, Russia. He graduated from the Kharkiv Engineering-Building Institute in 1962, with a specialization in “heat and ventilation.” For more than 30 years, he worked in the All-Union Scientific Research Institute of Safety and Environment in the Mining and Metallurgical Industry (Krivoy Rog), where he was promoted from research assistant to the head of the laboratory of industrial ventilation. Since 1994, he has been professor at Belgorod State Technological University, named after V. G. Shukhov.

Dr. Nikolayevich is author of more than 300 scientific papers, more than 50 inventions, and several monographs, including “Air Dedusting at Plants of Mining and Concentration Complexes, Moscow, Russia: Nedra, 1972,” “Aspiration of Vapor and Dust Mixtures in Dedusting of Process Equipment, Kiev, Ukraine: Naukova Dumka, 1974,” “Air Suction and Dedusting in Production of Powders, Moscow, Russia: Metallurgy, 1981,” “Aerodynamic Basis of Aspiration, St. Petersburg, FL: Himizdat, 2005,” “Dedusting Ventilation, Belgorod, Russia: BSTU, 2010,” “Aerodynamics Antidust Ventilation, Saarbruchen, Germany: LAP Lambert, 2012,” and “Industrial Air Quality and Ventilation: Controlling Dust Emissions, Boca Raton, FL: CRC Press, 2014.”



Konstantin Ivanovich Logachev holds a doctorate in engineering and is professor at Belgorod State Technological University, Belgorod, Russia, where he has been working since 1995. He graduated from the Dnepropetrovsk State University in 1992, with a specialization in “hydroaerodynamics.”

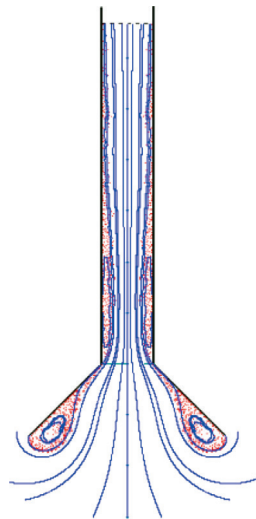
Dr. Ivanovich is author of more than 150 scientific publications, including many monographs: “Aerodynamics of Suction Torches, Belgorod, Russia: BSTU, 2000,” “Aerodynamic Basis of Aspiration, St. Petersburg, FL: Himizdat, 2005,” “Dedusting Ventilation, Belgorod, Russia: BSTU, 2010,” “Aerodynamics Antidust Ventilation, Saarbruchen, Germany: LAP Lambert, 2012,” and “Industrial Air Quality and Ventilation: Controlling Dust Emissions, Boca Raton, FL: CRC Press, 2014.”



Olga Aleksandrovna Averkova received a Candidate of Technical Sciences degree from Belgorod State Technological University, Belgorod, Russia, in 2004 and has been associate professor in that university since then. She is author of more than 100 scientific publications, including some monographs: “Dedusting Ventilation, Belgorod, Russia: BSTU, 2010” and “Aerodynamics Antidust Ventilation, Saarbruchen, Germany: LAP Lambert, 2012.”

Section I

Aerodynamics of Dust Airflows in the Spectra of Air Exhaust Ducts



I.1 INTRODUCTION

One of the main causes of occupational diseases in workers is emissions of dust, pollutants, heat, and water vapor that are inherent to production processes in the metal, mining, and chemical industries and building material production and other industries. Levels of harmful contaminants in the atmosphere of industrial premises are usually much higher than in the atmosphere of the adjacent areas. The adverse impact on the workplace affects a lot of people comprising the active working-age part of the population.

It is important to keep up workers' health not only socially, but also economically. Treatment of occupational diseases in workers costs to the state much more than the introduction of ventilation systems. In addition, when penetrating into the moving parts of equipment, dust contributes to their early wear that results in the deterioration of operational performance and output quality.

The most reliable way to control emissions of harmful substances is local exhaust ventilation. Despite the continuous increase in the cost of manufacturing, installation, and operation of local ventilation systems, their efficiency often remains poor. The adequate dimensioning of local suction units will reduce the dust level in the working area below the allowable concentration with the minimum exhaust air volumes, which is directly related to the power consumption of the hood exhaust system. This, in the era of energy crisis, is becoming of particular importance. Therefore, increasing the range of suction flares of local suction units is an important scientific and technical problem, the solution of which will have a significant economic and social benefit: pollutant emissions will be contained with minimum energy consumption.

A right choice of local exhaust design and its location depends not only on production technology but also on the methods used to calculate dust and gas flows near suction inlets. The development of these calculation methods can be classified into three stages:

1. Construction of empirical relationships and absorption spectra
2. Determination of analytical formulas for the simple boundaries of air inflow to a suction unit
3. Numerical simulation of flows at local suction units

The first stage is associated with the research by V.V. Baturin, A.F. Bromley, A.S. Pruzner, Della Valle, Engels, Koop, Willert, and others [1–11].

To calculate the rectangular and circular cross sections of the suction intake, Della Valle proposed an empirical relationship:

$$Q = (10x^2 + A)v_x,$$

where

Q is the volume flow rate

A is the suction inlet area

v_x is the axial air velocity at a point located at distance x from the suction port

For the same inlets with a flange

$$Q = 0.75(10x^2 + A)v_x,$$

where the hole vs. flange areas ratio may range from 1:2 to 1:2.5.

Koop obtained a relationship for a round suction intake

$$v_x = v_o \cdot e^{-3.2 \cdot x/d},$$

where

d is the diameter of the suction inlet

v_o is the air suction velocity

For a rectangular inlet, the following formula is proposed:

$$v_x = v_o \cdot e^{-3.2 \cdot \frac{xU}{4A}},$$

where U is the perimeter.

Engels and Willert obtained a combined relationship for round and rectangular inlets:

$$\left\{ \begin{array}{l} \frac{v_x}{v_o} = \frac{(x/r_h)^{-1.6}}{1 + (x/r_h)^{-1.6}}, \quad x/r_h \leq 2, \\ \frac{v_x}{v_o} = \frac{(x/r_h)^{-1.7}}{1 + (x/r_h)^{-1.7}}, \quad x/r_h > 2, \end{array} \right.$$

where $r_h = A/U$ is the hydraulic radius.

For similar junction pipes with a flange

$$\left\{ \begin{array}{l} \frac{v_x}{v_o} = \frac{1.35(x/r_h)^{-1.45}}{1 + 1.35(x/r_h)^{-1.45}}, \quad x/r_h \leq 2, \\ \frac{v_x}{v_o} = \frac{2(x/r_h)^{-1.9}}{1 + 2(x/r_h)^{-1.9}}, \quad x/r_h > 2. \end{array} \right.$$

The inlet area relates to the flange area as 1:2.3.

Upon the processing of experimental findings, engineer A.S. Pruzner [4] proposed his empirical formulas. For square and circular inlets for $x/r_h \leq 2$

$$\frac{v_x}{0.95 \cdot v_{av} - v_x} = 0.8 \left(\frac{x}{r_h} \right)^{-1.4},$$

where v_{av} is the average speed in the suction inlet. For rectangular inlets,

$$\left\{ \begin{array}{l} \frac{v_x}{v_{av} - v_x} = 0.8 \left(\frac{x}{r_h} \right)^{-1.4}, \quad x/r_h \leq 2, \\ \frac{v_x}{v_{av} - v_x} = \left(\frac{x}{r_h} \right)^{-1.7}, \quad x/r_h > 2. \end{array} \right.$$

For circular inlets

$$\frac{v_x}{v_{av}} = \left(\frac{x}{r_h} \right)^{-2}, \quad x/r_h > 2.$$

For square inlets

$$\frac{v_x}{v_{av}} = \frac{4}{\pi} \left(\frac{x}{r_h} \right)^{-2}, \quad x/r_h > 2.$$

M.F. Bromley [5] built an absorption spectrum for a circular inlet with sharp edges based on taking the velocity field experimentally. The absorption spectra for rectangular inlets with sharp edges in various fume-extraction hoods are described in a book by V.V. Baturin [6] and in work [7]. Article [8] studies the absorption spectrum, the scope of what includes a plane.

The experimental data accumulated during the period under review was used 50 years later in works [9,10], which approximated the experimental velocity field as found by M.F. Bromley. A suction spectrum model for the local suction of a stone-cutting machine was built upon the mathematical treatment of the experiment data (findings from 435 points were processed); its sphere of effect including a plane of the stone to be cut, which was accounted for by overlapping the spectrum of the model and its mirror image.

An expression, which is a particular solution of the Laplace equation, can serve as the basis for the experimental data analysis:

$$\Phi = e^{ax+by+cz} \quad \text{for } a^2 + b^2 + c^2 \neq 0,$$

where Φ is the velocity potential that was used in [2].

The above methods can be applied to a narrow class of simple suction inlets that were studied experimentally. Objects more complex than a plane placed in a suction flare cause considerable difficulties in determining the desired velocity field.

Among the experimental methods, we can point the method of electrohydrodynamic analogy (EHDA), which can be named a semianalytic method that allows calculating flat potential flows with any boundaries of the air inflow. This method was applied by Professor I.N. Logachev to construct a velocity field in the suction flares of local suction of industrial baths [11]. A geometrically similar model of an industrial bath and adjacent enclosing structures (walls, floors, etc.) was plotted on resistance paper. The boundary conditions were implemented in a certain way and the flow velocity $v(x, y)$ was determined at a desired point of the model (x, y) :

$$v(x, y) = \frac{\Delta\varphi}{\Delta\varphi_\infty} v_\infty,$$

where

$\Delta\varphi$ is the maximum increment of the potential near a point with coordinates (x, y)

$\Delta\varphi_\infty$ is the maximum increment of the potential near any point of the free-stream flow

v_∞ is the free-stream flow velocity

EHDA was used to obtain adjustment coefficients for the installation of industrial baths in calculating the lateral suction units. The same method was used to find the velocity components at flow around the cylinder.

The second historical stage is connected with such scientists as I.I. Konyshev, G.D. Livshits, I.N. Logachev, G.M. Pozin, V.N. Posokhin, E.V. Sazonov, V.N. Taliev, I.A. Shepelev, and others who calculated the local suction using the methods of conformal mappings, flow superposition, magnetic and vortex analogy, generalized flow superposition method, as well as direct integration of the Laplace equation by the Fourier method [12–51].

The greatest difficulties in the application of the conformal mapping method (see Chapter 1) relate to finding a mapping function, which is not always defined (e.g., for multiply connected domains). However, after this stage has been successfully completed, simple tasks can be solved without using a powerful computer but using a calculator. Unfortunately, the conformal mapping method allows solving only plane problems.

To describe plane potential airflows, a graphical method [12] was used based on the flow superposition method where a complex flow is presented as the sum of the simple ones. In the beginning, we build flow lines of flow components. To this end, we integrate the equation

$$\frac{dx}{v_x} = \frac{dy}{v_y}.$$

We superpose one family of flow lines over another family to obtain a grid in which cell sides represent the velocity vectors in a certain scale. The diagonal of any cell represents the velocity vector value of the resulting flow in the same scale.

The graphic method in [18] is used to calculate the velocity field near a slot-type connection pipe with two mutually perpendicular enclosing surfaces, where the flow was replaced by a system of sinks that are symmetrical mappings of the main sink on the surfaces. Evidently, the graphical method is not as accurate as the conformal mapping method.

The method of sources (sinks) [6,12] was used to calculate, approximately, the velocities at the selected points of both plane and 3D flows. It is based on the fact that at a considerable distance from the local suction, the velocity value varies according to the laws of sink:

$$v = \frac{L}{4\pi r^2},$$

where

L is the exhausted airflow

r is the distance from the suction center to the selected point

For the plane case, the equation for the velocity is as follows

$$v = \frac{L}{2\pi r}.$$

The calculation data obtained by the method of sinks may differ significantly from the experimental data.

The methods of vortex and magnetic analogy [27,52] are used to calculate the suction inlets in an unlimited space. These methods are based on the fact that the air velocity field is identified with the flux density field of a semi-infinite solenoid or semi-infinite *film of vortices*. Using the Biot–Savart law, I.I. Konyshov obtained the formulas to calculate the axial air velocity for the circular, rectangular, triangular, and round variable cross sections of semi-infinite suction connections. The following formula was obtained for a round connection pipe with a radius r with a suction rate v_o at a distance z from the suction opening:

$$v = \frac{v_o}{2} \left(1 - \frac{z}{\sqrt{r^2 + z^2}} \right).$$

For a rectangular pipe with a size of $2a \times 2b$

$$v = \frac{2v_o}{\pi} \operatorname{arctg} \frac{ab}{z\sqrt{a^2 + b^2 + z^2}},$$

and for a regular triangle-shaped pipe with the side b

$$v = \frac{3v_0}{\pi} \operatorname{arctg} \left[\sqrt{3} \frac{\sqrt{\frac{1}{3}b^2 + z^2 - z}}{\sqrt{\frac{1}{3}b^2 + z^2 + 3z}} \right].$$

Works [28–32] used the flow superposition method (see Section 1.4) with suction hole integration of sinks to obtain formulas to calculate the axial velocity at the exhaust openings built into an infinite flat wall. Abroad, the flow superposition method was used to study the velocity field near a rectangular suction inlet [44]. That study did not result in such simple formulas as those obtained by I.A. Shepelev. The sources were integrated by summing up 100 single sinks. A flow confined by walls (one, two, and three mutually perpendicular walls) was studied and described using mirror-image presentation and graphical addition. This method was used to consider a problem in the plane [45] for a single point sink, a point source, and a plane flow.

E.V. Sazonov [50,51] offered new formulas to calculate the extension length of the projecting hood and the required volumes of aspiration to remove escaping gases at loading and unloading of electric furnaces on the basis of formulas by V.N. Posokhin, I.A. Shepelev, M.I. Grititlin [49], and the methodology [48].

Though the flow superposition method is more than simple, it is difficult to determine how to superpose the elementary flows to get a pattern of the flow of interest, especially when it comes to local suction units in confined conditions. In his work [53], N.Ya. Fabrikant describes the generalized flow superposition method, which enables to solve this problem. Sections 4 and 5 describe the principle of this method. We only note that it consists of solving the Fredholm second-order boundary integral equations. Therefore, abroad, this method was named the boundary integral equation method, or the boundary element method [54–57,59], based on the works by Russian mathematician S.G. Mikhlin [58]. The generalized flow superposition method is a special case of the BIE method, as the latter covers a wider class of problems, including elasticity problems.

The generalized flow superposition method, sometimes referred to as the method of *singularities* in the aerodynamics, was applied by G.D. Livshits and his followers [33–38,128] to calculate circular, square, and ring-type semi-infinite pipes that are loosely spaced. There are some similar studies abroad as well [46,47]. No calculation of flows with complex boundaries was made.

The third historical stage of development of calculation methods for local suction units is connected with an intensive development of computer technology and using IT software for numerical methods of aerohydrodynamics and mathematical analysis. We must mention the contributions made by V.K. Khrushch, N.N. Belyaev, V.G. Shaptala, G.L. Okuneva, V.N. Posokhin, I.L. Gurevich, R.Kh. Akhmadeev, I.I. Konyshv, and other researchers [60–78].

Work [60] investigates a slot-type suction unit from axially symmetric diffusion sources (a ring-type suction unit from a round bath). It provided the solution of the continuity equation for the potential flow in cylindrical coordinate system r, z :

$$\frac{\partial^2 \psi}{\partial z^2} + \frac{\partial^2 \psi}{\partial r^2} - \frac{1}{r} \frac{\partial \psi}{\partial r} = 0,$$

where ψ is the flow function.

This equation was approximated using a five-point stencil and was solved by the Seidel iterative method combined with the overrelaxation method. After that, velocity components were calculated using difference analogues.

I.I. Konyshv proposed a computation algorithm for axially symmetric problems by the numerical integration of the Laplace equation in a spherical coordinate system by the method of finite differences.

An axially symmetric flow at a circular flanged pipe is studied in [61]. The velocity field was also based on the numerical integration of the Laplace equation.

Works [70,71] model flat airflows in a production room when it is ventilated with jets. Here, we have used a vorticity transfer and diffusion equation obtained from the Navier–Stokes equation in the Boussinesq approximation and the Poisson equation for the flow function

$$\frac{\partial \Omega}{\partial t} + \nabla \cdot (\bar{v} \Omega) = \frac{1}{\text{Re}_t} \Delta \Omega,$$

$$\Delta \psi = -\Omega,$$

where \bar{v} is the time-averaged dimensionless air velocity value. The vorticity vector is

$$\Omega = \frac{\partial v_y}{\partial x} - \frac{\partial v_x}{\partial y}.$$

The horizontal and vertical components of velocity are

$$v_x = \frac{\partial \psi}{\partial y}, \quad v_y = -\frac{\partial \psi}{\partial x},$$

where ψ is the flow function. The Reynolds number was defined by the relation

$$\text{Re}_t = 5 \frac{v_1 H}{vl} \sqrt[3]{\frac{HD}{l^2}},$$

where

$$v_1 = 1 \text{ m/s}$$

H, D are the height and width of the room

l is the basic scale of turbulence

The explicit conservative Arakawa scheme was used to solve the vorticity transfer equation. The successive overrelaxation scheme was used to solve the Poisson equation by the relaxation method.

Simulation of distribution of airflows, temperature, and concentration of impurities in the workplace was performed in [72,75,76] on the basis of the Navier–Stokes equations in the Boussinesq–Oberbeck approximation, equations of heat transfer, and convective diffusion of impurities. The numerical solution of these equations served as a base to study, by the relaxation method, the foundry shake-out department aspiration system that consists of a local exhaust unit and general dilution airflow [73,74].

A software system (SS) *Aspiration* developed by V.K. Khrushch and N.N. Belyaev determines the optimal location of local suction units and aspirated air volumes [77,78] that helps to

ensure the greatest concentration of impurities in the exhaust air. The Aspiration SS is based on a numerical integration of the equation

$$\begin{aligned} & \frac{\partial \varphi}{\partial t} + \frac{\partial u \varphi}{\partial x} + \frac{\partial v \varphi}{\partial y} + \frac{\partial (w - w_s) \varphi}{\partial z} + \sigma \varphi \\ & = \operatorname{div}(\mu \nabla \varphi) + \sum_{i=1}^N q_i(t) \delta(r - r_i(t)) - \sum_{j=1}^M \varphi Q_j(t) \delta(r - r_j), \end{aligned}$$

where

$q_i(t)$ is the strength of a point source of pollutant emissions

$r_i(x_i, y_i, z_i)$ are the Cartesian coordinates of the specified source

Q_j is the airflow removed by the local suction, which is presented as a 3D point sink in this model

$\delta(r - r_i), \delta(r - r_j)$ are the deltas of the Dirac function

φ is the concentration of pollution

u, v, w are the air velocity projections

w_s is the rate of gravitational sedimentation of contaminants

The most promising method [16,117,126, Chapter 3] currently is the method of discrete vortices [79,112,113,130–141], which is widely used in aerodynamics to calculate bearing surfaces, turbulent jets, and wakes. This method applied to problems of airflows near the suction holes [80,82–88,93,94] enables not only to take into account the formation of transient eddy zones, but also to investigate the interaction of supply air jets and suction flares.

Stochastic and deterministic methods are used to calculate the dynamics of the solids in ventilating air jets in an unlimited and confined space. Considerable computational effort is required to describe the dispersed phase on the basis of the kinetic equation for the one-particle distribution function [142]. The deterministic method based on the discrete vortex method is used to calculate the distribution of dispersed particles in turbulent jets and aircraft trail [116]. Work [104] offers a method to forecast the dispersed composition of the dust particles in the aspirated air at the transshipment of bulk materials on the basis of the method of trajectories and determination of the maximum diameter of dust particles. The value of the maximum diameter was assumed to be the reference point and the particle size distribution was assumed to adhere to the lognormal distribution. Note that the definition of the particle size distribution and concentration of dust particles in the aspirated air is a difficult and ambiguous problem in experimental aerodynamics as well. The experimental results vary in a quite large range and sometimes contradict each other due to the pulsation nature of processes.

1 Determination of the Velocity Field by Conformal Mapping Methods

1.1 UNSEPARATED FLOWS

1.1.1 GENERAL INFORMATION ON THE CONFORMAL MAPPING METHOD

A mapping of the area z on the area ω , as defined by the function $\omega = f(z)$, is called conformal if it preserves the stretches and rotation angles. This means that any infinitesimally small element in z varies the same number of times as it is mapped $\omega = f(z)$ and the linear expansion coefficient is $|f'(z)|$. The curve in the area z is rotated by the same angle $\alpha = \arg f'(z)$ in the same direction when mapped $\omega = f(z)$. Conformal mapping method is used to calculate the potential flows of gas. A flow is called potential if there is a function φ that is called a potential, for which the following equality is true:

$$\vec{v} = \text{grad } \varphi, \quad (1.1)$$

where \vec{v} is the flow velocity.

The horizontal and vertical components of velocity are determined, respectively, by the formulas

$$v_x = \frac{\partial \varphi}{\partial x}, \quad v_y = \frac{\partial \varphi}{\partial y}. \quad (1.2)$$

The continuity equation for a flat potential flow of gas is reduced to the Laplace equation for the potential

$$\frac{\partial v_x}{\partial x} + \frac{\partial v_y}{\partial y} = \frac{\partial^2 \varphi}{\partial x^2} + \frac{\partial^2 \varphi}{\partial y^2} = 0. \quad (1.3)$$

The line on which $\varphi = \text{const}$ is called an equipotential.

In addition to the potential, a flow function ψ is introduced:

$$v_x = \frac{\partial \psi}{\partial y}, \quad v_y = -\frac{\partial \psi}{\partial x}, \quad (1.4)$$

which also satisfies the continuity equation.

The line on which the function ψ is constant is called a flow line. The velocity vector is tangential at each point of the flow line. The equipotentials and flow lines are mutually perpendicular.

The complex flow potential is the function

$$w = \varphi + i\psi. \quad (1.5)$$

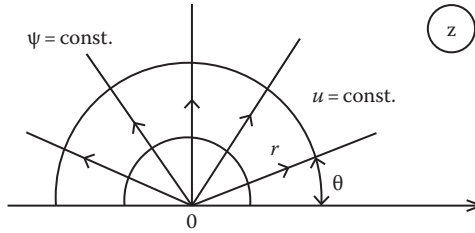


FIGURE 1.1 Point source in the semiplane.

If we know the function w in the flow plane z , then by defining the complex velocity

$$\frac{dw}{dz} = \frac{\partial w}{\partial x} \frac{\partial x}{\partial z} = \frac{\partial \varphi}{\partial x} + i \frac{\partial \psi}{\partial x} = v_x - i v_y, \quad (1.6)$$

we can find the vertical and horizontal components of the velocity at any point in the flow range.

Define, for example, the complex flow potential in the upper semiplane with a point source of a strength Q located in the origin of coordinates (Figure 1.1).

In this case, the flow lines are rays starting at 0 and the equipotentials are semicircumferences. The velocity along the flow line is

$$v_r = \frac{\partial \varphi}{\partial r} = \frac{Q}{\pi r}, \quad (1.7)$$

whence $\varphi = \int \frac{Q}{\pi r} dr = \frac{Q}{\pi} \ln r + C$. Assume that $\varphi = 0$ for $r = 1$, then $C = 0$. In order to determine the flow function, we calculate its partial derivative:

$$\frac{\partial \psi}{\partial y} = v_x = v_r \cos \theta = \frac{Qx}{\pi r^2}. \quad (1.8)$$

For the first quadrant, the angle $\theta = \arctg \frac{y}{x}$ and for the second one, it is $\theta = \pi + \arctg \frac{y}{x}$. Therefore, $\frac{\partial \theta}{\partial y} = \frac{x}{r^2}$. As $\frac{d\psi}{d\theta} = \frac{\partial \psi}{\partial y} \frac{\partial y}{\partial \theta} = \frac{Q}{\pi}$, $\psi = \frac{Q}{\pi} \theta$ (const = 0, as we choose $\psi = 0$ for $\theta = 0$) and the complex potential is $w = \frac{Q}{\pi} \ln r + i \frac{Q}{\pi} \theta = \frac{Q}{\pi} \ln z$. If the point source is at the point z_0 , then

$$w = \frac{Q}{\pi} \ln(z - z_0). \quad (1.9)$$

In the case of a point sink

$$w = -\frac{Q}{\pi} \ln(z - z_0). \quad (1.10)$$

The algorithm for calculating the gas velocity field in a given flow plane that is called a physical plane consists of the following steps:

1. Definition of the mapping of the physical flow plane z onto the upper semiplane t (a geometric flow plane, which can be represented by any other area with a known complex potential):

$$z = f(t). \tag{1.11}$$

2. Setting the point z_0 , in which it is necessary to determine the flow rate, and calculating the parameter t_0 by Equation 1.11.
3. Calculation of the complex velocity

$$\frac{dw}{dz} = \frac{dw}{dt} \frac{dt}{dz}, \tag{1.12}$$

which is used to determine the coordinates of the velocity vector.

Step 1 is the most demanding one. In addition, mapping Equation 1.11 cannot be defined for multiply connected regions, which are not reduced to simply connected ones, and, therefore, the conformal mapping method cannot be applied for such problems.

An important property of conformal mappings is the principle of symmetry. If a certain line divides the physical flow area into two symmetric subareas, then one of them can be disregarded and the velocity field can be calculated for the remaining subarea. The obtained calculation results of the velocity field will be valid for the symmetric points of the disregarded subarea as well.

Consider the mapping of the upper semiplane onto the interior of a polygon (Figures 1.2 and 1.3), which is often used in engineering practice [89].

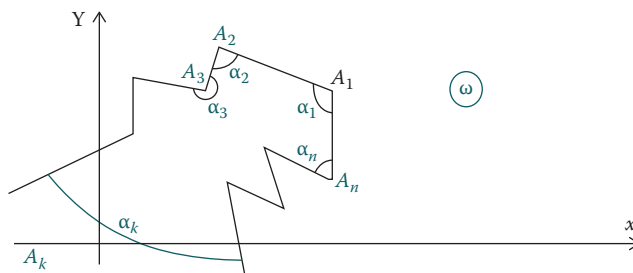


FIGURE 1.2 Polygonal domain.

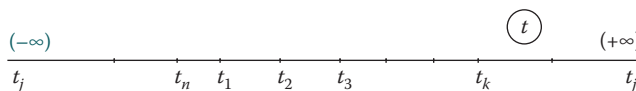


FIGURE 1.3 Upper semiplane.

The sense of the area traversal is chosen so that the area is always on the left if we move counter-clockwise along the area boundary. The upper semiplane on a polygonal area is mapped using the Schwarz–Christoffel formula:

$$\omega = C_1 \int_{t_k}^t (t - t_1)^{\frac{\alpha_1}{\pi} - 1} (t - t_2)^{\frac{\alpha_2}{\pi} - 1} \dots (t - t_n)^{\frac{\alpha_n}{\pi} - 1} dt + C_2, \tag{1.13}$$

where

- t_1, t_2, \dots, t_n are n independent parameters
- $\alpha_1, \alpha_2, \dots, \alpha_{n-1}$ are $(n - 1)$ independent parameters
- $\alpha_1 + \alpha_2 + \dots + \alpha_{n-1} + \alpha_n = (n - 2)\pi$
- C_1, C_2 are complex constants, and, therefore, four independent parameters

In total, we have $2n + 3$ independent parameters. Note that if t_j is in ∞ , then the integral does not contain the term $(t - t_j)^{\frac{\alpha_j}{\pi} - 1}$. When mapping by the Schwarz–Christoffel formula, with the preserved sense of traversal, the abscissas in three points in the plane t can be arbitrarily set and the remaining ones must be defined. The reference point t_k is assigned in such a way that the constant C_2 could be easily determined.

1.1.2 CALCULATION OF THE AXIAL AIR VELOCITY AT A FREELY SPACED SLOT-TYPE SUCTION

Direct the axis OX along the symmetry axis of the slot-type opening with a width of $2B$ with an air exhaust rate on ∞ equal to 1 (Figure 1.4). Define the air velocity on the axis OX .

Since this area is symmetrical about the horizontal axis, the lower part of the figure can be disregarded (Figure 1.5).

Map the upper semiplane (Figure 1.6) onto the resulting triangular area (Figure 1.5). The points A_1, A_2, A_3 are mapped, respectively, onto t_1, t_2, t_3 .

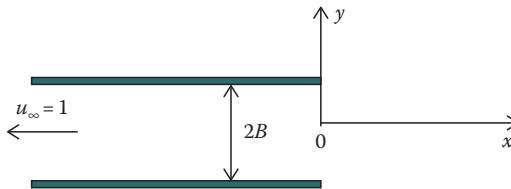


FIGURE 1.4 Freely spaced slot-type suction.

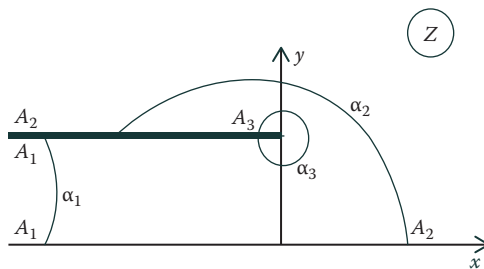


FIGURE 1.5 Physical flow plane.

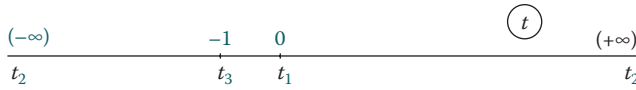


FIGURE 1.6 Geometric flow plane.

The angles $\alpha_1 = 0$, $\alpha_3 = 2\pi$. As $\alpha_1 + \alpha_2 + \alpha_3 = \pi \Rightarrow \alpha_2 = \pi - 2\pi = -\pi$.
 The Schwarz–Christoffel integral for this mapping is

$$z = C_1 \int_{t_k}^t (t-0)^{0-1} (t+1)^{\frac{2\pi-1}{\pi}} dt + C_2. \tag{1.14}$$

We recommend choosing as a reference point t_k such a point that allows easily determining the constant C_2 . In this case, $t_k = t_3 = -1$. Then,

$$z = C_1 \int_{-1}^t \frac{t+1}{t} dt + C_2. \tag{1.15}$$

If we assume $t = -1$, then $z = iB$ and $C_2 = iB$. The constant C_1 is determined from the correspondence of the points A_1 and t_1 . We use the fact that in going through the point t_1 along an infinitely small circle with a radius ε from the ray $t_1 t_2$ to the interval $t_1 t_3$, a jump of iB from $A_1 A_2$ to $A_1 A_3$ in the plane z occurs, that is,

$$z(+\varepsilon) - z(-\varepsilon) = 0 - iB = -iB. \tag{1.16}$$

We integrate Equation 1.15 to obtain

$$z = C_1(t + 1 + \ln t - i\pi) + iB.$$

Let us calculate the values of z at the points ε and $-\varepsilon$ when $\varepsilon \rightarrow 0$:

$$z(\varepsilon) = C_1(\varepsilon + 1 + \ln \varepsilon - i\pi) + iB$$

$$z(-\varepsilon) = C_1(-\varepsilon + 1 + \ln \varepsilon + i\pi - i\pi) + iB.$$

Therefore,

$$\lim_{\varepsilon \rightarrow 0} (z(\varepsilon) - z(-\varepsilon)) = -i\pi C_1.$$

Use Equation 1.16 to define

$$-iB = -i\pi C_1 \Rightarrow C_1 = \frac{B}{\pi}.$$

Thus, the desired mapping is

$$z = \frac{B}{\pi}(t + 1 + \ln t). \tag{1.17}$$

TABLE 1.1**Values of the Axial Velocity of Air Inflow to the Slot-Type Suction Unit in an Infinite Space**

x/B	0	0.5	1	1.5	2	2.5	3	3.5	4	4.5	5
u	0.78	0.56	0.38	0.27	0.2	0.16	0.13	0.11	0.1	0.09	0.08

On the flow geometric plane (Figure 1.6), we have a point sink at the point t_1 . Therefore, the complex potential of this flow is $w = -(Q/\pi)\ln t$. The complex velocity in the physical plane (Figure 1.5) is

$$\frac{dw}{dz} = \frac{dw}{dt} \frac{dt}{dz} = -\frac{1}{t+1}.$$

Thus, the algorithm for calculating the axial velocity at a freely spaced slot-type suction unit consists of four steps (Table 1.1):

1. The initial coordinate $x = 0$ is preset.
2. The formula $x = \frac{B}{\pi}(1 + t + \ln t)$ is used to determine the parameter t , for example, by the half-interval method.
3. The formula $u_x = -\frac{1}{t+1}$ is used to calculate the axial velocity of the air at x .
4. Perform the step $x = x + \Delta x$ and return to Step 2. Calculate until the predetermined point is reached.

1.1.3 CALCULATION OF THE AXIAL AIR VELOCITY AT SLOT-TYPE SUCTION BUILT IN A FLAT INFINITE WALL

Similar to Section 1.2, we assume that the width of the slot-type opening is $2B$ and the suction velocity $u_\infty = 1$ (Figure 1.7). Define the air inflow velocity on the horizontal axis.

As the flow area is symmetric, we can disregard the lower semiplane (Figure 1.8).

The geometric flow plane (Figure 1.9) is mapped onto a physical one with the Schwarz–Christoffel formula:

$$z = C_1 \int_0^t \frac{\sqrt{t}}{t-1} dt + C_2. \quad (1.18)$$

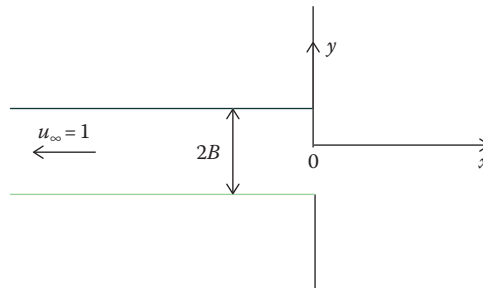


FIGURE 1.7 Slot-type suction built in a flat infinite wall.

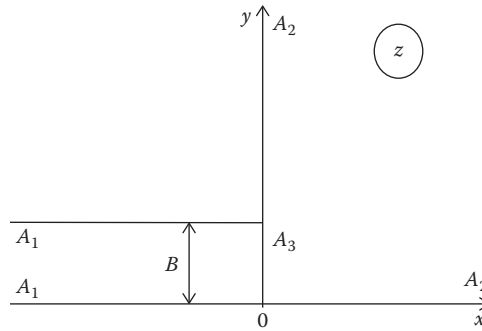


FIGURE 1.8 Physical flow plane.

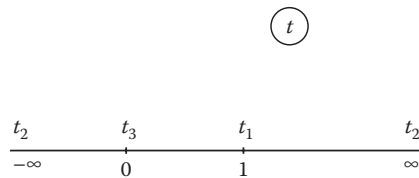


FIGURE 1.9 Geometric flow plane.

The constant $C_2 = iB$, as $z = iB$ for $t = 0$. On integrating expression Equation 1.18 we obtain

$$z = C_1 \left[2\sqrt{t} + \ln \left(\frac{\sqrt{t} - 1}{\sqrt{t} + 1} \right) - i\pi \right] + iB. \tag{1.19}$$

The constant C_1 is determined from the correspondence of the points t_1 and A_1 . When the point t_1 is traversed along the semicircle of the radius $\varepsilon \rightarrow 0$ from the ray $t_1 t_2$ to the interval $t_3 t_1$, a jump in the physical plane occurs at $\Delta z = -iB$.

As $\lim_{\varepsilon \rightarrow 0} [z(1 + \varepsilon) - z(1 - \varepsilon)] = -C_1 \cdot i\pi \Rightarrow C_1 = \frac{B}{\pi}$, the desired mapping will be

$$z = \frac{B}{\pi} \left[2\sqrt{t} + \ln \frac{\sqrt{t} - 1}{\sqrt{t} + 1} \right]. \tag{1.20}$$

The complex flow potential on the geometrical plane is $w = -(Q/\pi)\ln(t - 1)$, so the complex velocity is

$$\frac{dw}{dz} = \frac{dw}{dt} \frac{dt}{dz} = -\frac{1}{\sqrt{t}}. \tag{1.21}$$

The calculation algorithm consists of the following steps:

1. The initial coordinate $x = 0$ is preset.
2. The formula $x = \frac{B}{\pi} \left(\sqrt{t} + \ln \frac{\sqrt{t} - 1}{\sqrt{t} + 1} \right)$ is used to determine the parameter t .
3. The formula $u_x = -\frac{1}{\sqrt{t}}$ is used to calculate the axial velocity of the air at x .
4. Perform the step $x = x + \Delta x$ and return to Step 2. Calculate until the predetermined point is reached.

TABLE 1.2
Values of the Axial Velocity of Air Inflow to the Slot-Type Suction Unit Built in a Flat Infinite Wall

x/B	0	0.5	1	1.5	2	2.5	3	3.5	4	4.5	5
u	0.83	0.65	0.48	0.37	0.29	0.24	0.2	0.18	0.16	0.14	0.13

The calculation results (Tables 1.1 and 1.2) show that the axial velocity at a slot-type suction unit built into the flat infinite wall is higher than at a freely spaced suction; this can be explained by the influence of the gas inflow boundaries. In the first case, the inflow region is smaller than in the second one. Note that if the air suction rate $u_\infty \neq 1$, then all the results obtained should be multiplied by this value.

1.1.4 CALCULATION OF THE AXIAL AIR VELOCITY AT A SLOT-TYPE SUCTION BELL

Local suction hoods are widely used in containing ventilation. It can be useful to find the optimal length and tilting angle of the hood bell that ensure the maximum range of local suction intake flare. The range of the intake flare refers to the distance from the suction entrance to the point where the axial velocity equals a predetermined value.

Consider the airflow near a slot-type suction with a width $2B$ having a flange (hood) of length l , which is mounted at an angle $\alpha\pi$ ($-1 < \alpha < 1$) to its axis (Figure 1.10). Determine the dependence of the axial velocity v_ξ on the angle $\alpha\pi$ and the flange length l .

The Schwarz–Christoffel formula is used to map the upper semiplane z onto the physical plane ω with the point correspondence as shown in Figures 1.10 and 1.11:

$$\omega = \frac{Bm^\alpha}{\pi b} \int_{-1}^z \left(\frac{t+1}{t+m} \right)^\alpha \left(\frac{t+b}{t} \right) dt + Bi. \tag{1.22}$$

The complex flow potential in the upper semiplane (the sink is at the point a_1 , the source is at a_2)

$$w = -\frac{Q}{\pi} \ln z, \tag{1.23}$$

where $Q = v_\infty B$ is the airflow and the complex velocity is

$$\frac{dw}{dz} = -\frac{Q}{\pi z}. \tag{1.24}$$

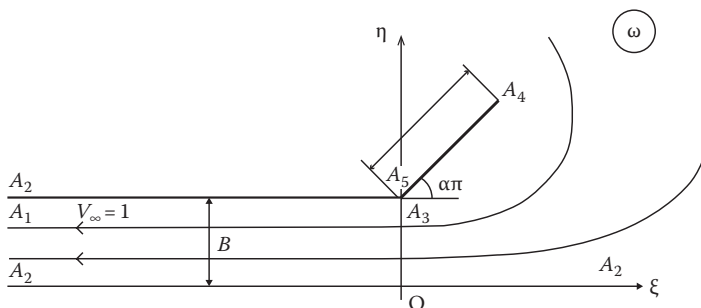


FIGURE 1.10 Air inflow to a freely spaced slot-type flanged pipe.

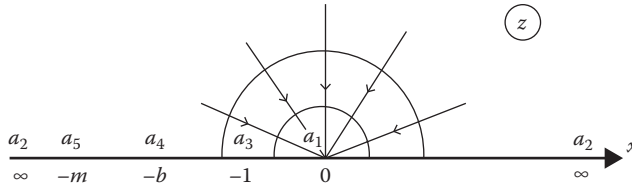


FIGURE 1.11 Sink in the upper semiplane.

The complex velocity in ω can be found using the equation $v(\omega) = \frac{dw}{d\omega} = \frac{dw}{dz} \frac{dz}{d\omega}$ and formula (Equation 1.22):

$$v(\omega) = -\frac{Qb(z+m)^\alpha}{Bm^\alpha(z+1)^\alpha(z+b)}. \tag{1.25}$$

The axial velocity of the slot-type suction (at 0ξ) is determined from the equality

$$-\frac{v_\xi}{v_\infty} = \frac{b}{m^\alpha} \left(\frac{x+m}{x+1} \right)^\alpha \frac{1}{x+b}. \tag{1.26}$$

Relations (Equations 1.22 and 1.26) are formally the solution of the problem set.

The unknown parameters m, b in Equation 1.22 are determined based on the correspondence of the points A_4, A_5 and a_4, a_5 (Figures 1.10 and 1.11) by setting the values of the flange length l/B and the angle α :

$$\int_1^m \left(\frac{t-1}{m-t} \right) dt - b \int_1^m \left(\frac{t-1}{m-t} \right)^\alpha \frac{dt}{t} = 0, \tag{1.27}$$

$$\frac{l\pi b}{Bm^\alpha} = \int_1^b \left(\frac{t-1}{m-t} \right)^\alpha \frac{b-t}{t} dt. \tag{1.28}$$

The integrals in Equations 1.27 and 1.28 were calculated by the Gauss quadrature formulas. However, the difficulties in solving this problem extend much further. The integral in Equation 1.22 is convergent only in the sense of the principal value (integral of Cauchy type). It is difficult to find the numerical value of this integral. Thus, we reduce Equation 1.22 to a form more suitable for numerical integration.

Since we are only interested in points on the axis of suction, then $z = x$ in Equation 1.22, in which the integral is transformed as follows:

$$J = \int_{-1}^x \left(\frac{t+1}{t+m} \right)^\alpha \frac{t+b}{t} dt = bJ_1 + (1-b)J_2,$$

where $J_2 = \int_{-1}^x \left(\frac{t+1}{t+m} \right)^\alpha$ is a convergent integral for $\alpha > -1$ and the integral $J_1 = \int_{-1}^x \frac{(t+1)^{\alpha+1}}{(t+m)^\alpha} \frac{dt}{t}$ is

divided into three: $J_1 = \int_{-1}^{-\epsilon} + \int_{-\epsilon}^{\epsilon} + \int_{\epsilon}^x \epsilon \rightarrow 0$.

The integration paths of the first and third integrals are straight-line segments of the real axis and are definite integrals of the real function. The second integral is integrated over the semicircle with a radius $r = \varepsilon$ centered at a_1 (see Figure 1.11):

$$\int_{-\varepsilon}^{\varepsilon} \frac{(t+1)^{\alpha+1}}{(t+m)^{\alpha}} \frac{dt}{t} = \int_{\pi}^0 \frac{(re^{i\varphi} + 1)^{\alpha+1}}{(re^{i\varphi} + m)^{\alpha}} \frac{ire^{i\varphi}}{re^{i\varphi}} d\varphi = \{r = \varepsilon \rightarrow 0\} = \frac{-\pi i}{m^{\alpha}}.$$

Using the integration formula by parts, define

$$J_1 = \frac{(1+x)^{\alpha}}{(m+x)^{\alpha}} (1+x) \ln x + \alpha(1-m) \int_{-1}^x \left(\frac{1+t}{m+t} \right)^{\alpha} \frac{\ln|t|}{m+t} dt - \int_{-1}^x \left(\frac{1+t}{m+t} \right)^{\alpha} \ln|t| dt - \frac{\pi i}{m^{\alpha}}$$

and after substituting the obtained value J_1 in Equation 1.22, we have

$$\omega = \frac{Bm^{\alpha}}{\pi b} \left[b \frac{(1+x)^{\alpha+1}}{(m+x)^{\alpha}} + b\alpha(1-m)I_1 - bI_2 + (1-b)I_3 \right], \quad (1.29)$$

where

$$I_1 = \int_{-1}^x \left(\frac{1+t}{m+t} \right)^{\alpha} \frac{\ln|t|}{m+t} dt$$

$$I_2 = \int_{-1}^x \left(\frac{1+t}{m+t} \right)^{\alpha} \ln|t| dt$$

$$I_3 = \int_{-1}^x \left(\frac{t+1}{t+m} \right)^{\alpha} dt$$

The integrals I_1, I_2, I_3 are convergent improper integrals [102] for $\alpha > -1$.

The algorithm for determining the axial velocity consists of four steps:

1. We assign the value of the flange length l/B , flange tilt angle α , and the coordinates of the point on the slot axis ξ/B (and at each time the distance is measured from the flange edge, i.e., from the abscissa of the point A, i.e., for $0.5 < \alpha < 0.5$, the point coordinates are $\xi/B + l/\cos \alpha$).
2. We calculate the parameters m and b from Equations 1.27 and 1.28.
3. Use Equation 1.29 to determine the parameter x .
4. Use Equation 1.26 to determine the axial velocity v_{ξ}/v_{∞} .

The calculations have shown that the axial velocity at the suction slot with a flange of a finite length has three extrema (Figure 1.12) when the flange tilt angle changes within $-1 < \alpha < 1$, of which two maximums are at $\alpha = 0.5$ and $\alpha = -0.5$.

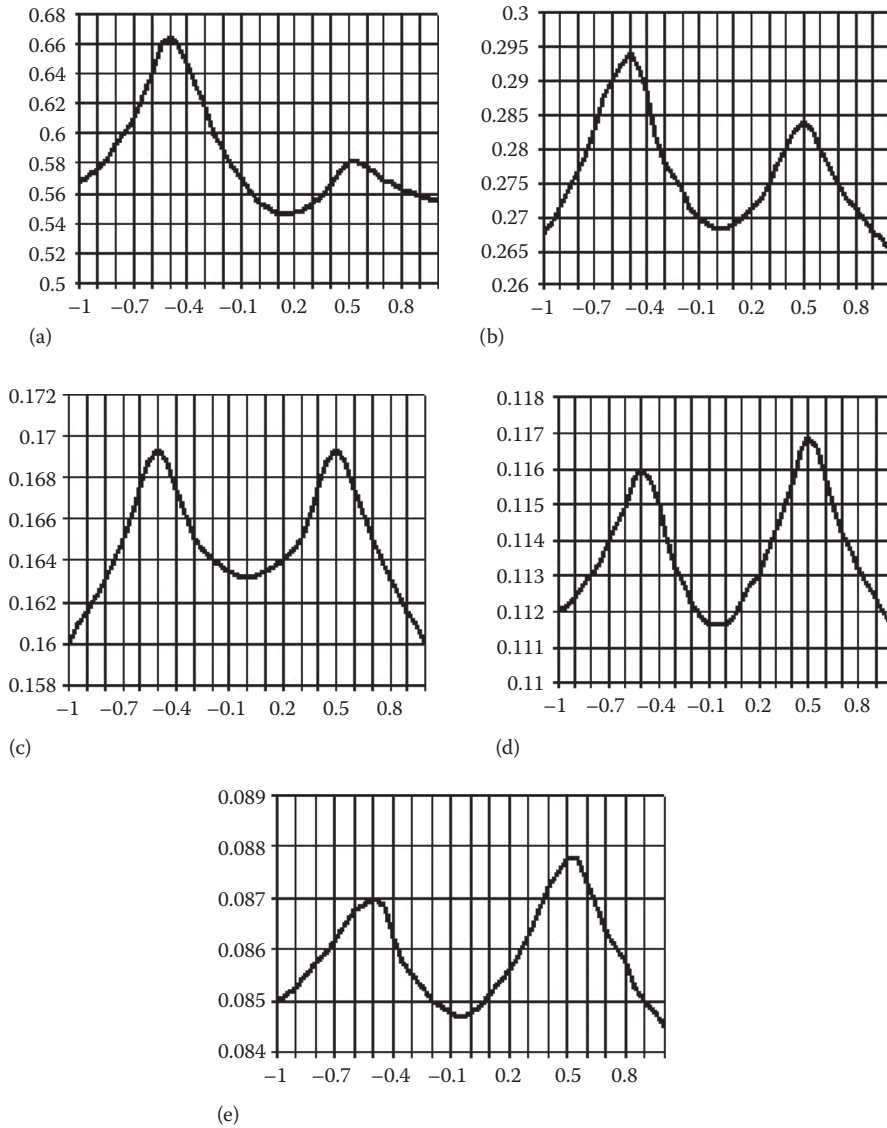


FIGURE 1.12 Change in the axial velocity v_{ξ}/v_{∞} (vertical axis) as a function of the flange tilt angle α (horizontal axis) at the fixed point ξ/B : (a) $\xi/B = 0.5$, (b) $\xi/B = 1.5$, (c) $\xi/B = 2.5$, (d) $\xi/B = 3.5$, and (e) $\xi/B = 4.5$.

In this case, the greatest value of the axial velocity is found at a distance $0 < \xi/B < 2.5$ from the entry section for $\alpha = -0.5$ and in $\xi/B > 2.5$ for $\alpha = 0.5$.

The range of the suction flare increases with the increase in flange length (Figure 1.13). In the area $\xi/B < 3$, the axial velocity for $l/B = 3$ almost reaches its limit (corresponding to $l/B \rightarrow \infty$).

The results obtained confirm the well-known fact that the flow boundaries play the dominant role. In our case, the boundaries are the flange and walls of the suction channel. The role of the former is essential for the flow near the suction section, but the suction channel walls have a greater influence at a considerable distance. The regular change in the axial velocity follows the law of the line sink in the latter case.

Despite that the maximum axial velocity in $\xi/B < 2.5$ is observed when $\alpha = -0.5$; it is not advisable to install the flange at a negative angle due to an increase in power consumption resulting from an increase in the velocity of air entry into the suction channel, which would be inevitable in this case.

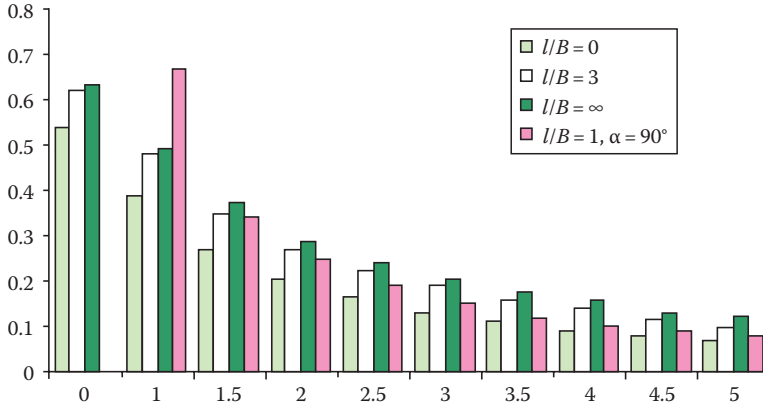


FIGURE 1.13 Change in the axial velocity v_z/v_∞ (vertical axis) as a function of the distance from the suction entrance ξ/B (horizontal axis).

Thus, we plotted the dependence of the axial velocity of the open-type slotted suction on the length and tilt angle of its hood (flange). The least axial velocity attenuation is achieved when the flange is installed at the right angle to the axis of the slot whose optimal length is three gauges (a gauge is a half-width of the slot).

1.2 SEPARATED FLOWS

We will assume the following classical assumptions used to calculate the sucked airflows [16,89]: the liquid is weightless and incompressible, no vortex is present, and the flow is steady. The normal component of velocity on the solid walls and unknown free flow lines (resulting from the separation of the flow) is equal to zero. In addition, the module of velocity u_0 is constant on free flow lines. In the described approach, the free flow line is the boundary between the vortex region, occurring at the walls, and a potential flow that will be studied. It follows that a flow is determined if the velocity potential $w(z)$ is known where $z = x + iy$ is a physical plane of the airflow.

The Joukowski function is as follows:

$$\omega = -\ln \frac{dw}{u_0 dz} = -\ln \frac{u_x - iu_y}{u_0} = -\ln \frac{u(\cos\theta - i\sin\theta)}{u_0} = -\ln \left(\frac{u}{u_0} e^{-i\theta} \right) = -\ln \frac{u}{u_0} + i\theta, \quad (1.30)$$

where θ is the angle of the velocity vector \vec{u} to the positive direction of the axis OX .

The plane of the Joukowski function ω must be mapped on the parametric plane t where the complex potential of the flow is known, and then this parametric plane t must be linked with the physical plane z . If the mapping $\omega = \omega(t)$ is known, then we use the expression $\omega(t) = -\ln(dw/u_0 dz)$ to determine that

$$z = \frac{1}{u_0} \int e^{\omega(t)} \frac{dw}{dt} dt. \quad (1.31)$$

Use this formula to find the desired complex velocity:

$$\frac{dw}{dz} = \frac{dw}{dt} \frac{dt}{dz} = u_0 e^{-\omega(t)}. \quad (1.32)$$

1.2.1 CALCULATION OF THE AIRFLOW AT THE SLOT-TYPE SUCTION BUILT IN A FLAT INFINITE WALL

Let the air from the half space $x > 0$ go into the slotted opening with a width $2B$. The flow is separated from the edges of the suction unit. The problem consists of determining the width of the potential flow 2δ for $x \rightarrow -\infty$ and the air velocity on the axis OX (Figure 1.14).

As the flow range is symmetric, we can disregard the lower semiplane (Figure 1.15).

On the line A_1A_2 , the velocity varies from 0 to u_0 and the angle $\theta = -\pi/2$ is constant. The real part of the Joukowski function $\text{Re } \omega$ decreases here from ∞ to 0, the imaginary part is $\text{Im } \omega = -\pi/2$. On A_2A_3 , the velocity is constant and equal to u_0 and the velocity angle θ varies from $-\pi/2$ to $-\pi$, that is, $\text{Re } \omega = 0$ and $\text{Im } \omega$ decreases from $-\pi/2$ to $-\pi$. On the line A_3A_1 , the velocity decreases from u_0 down to 0 ($\text{Re } \omega$ increases from 0 up to ∞) and the angle $\theta = \text{Im } \omega = -\pi$ is constant. Thus, the area of the Joukowski function is a semiband (Figure 1.16).

Map the area of the Joukowski function on the parametric plane t (Figure 1.16) using the Schwarz–Christoffel formula:

$$\omega = C_1 \int_{-1}^t \frac{dt}{\sqrt{t+1}\sqrt{t}} + C_2, \tag{1.33}$$

where $C_2 = -\pi/2 \cdot i$, as for $t = -1 \Rightarrow \omega = -\pi/2 \cdot i$.

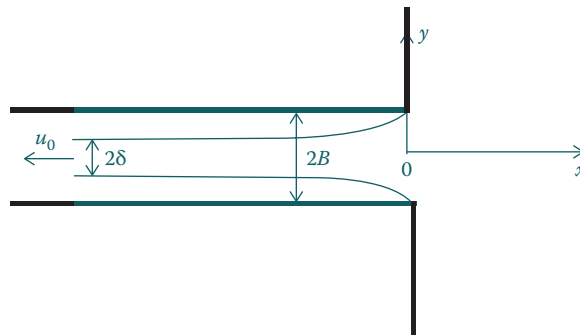


FIGURE 1.14 Separated airflow at the slot-type suction built in a flat infinite wall.

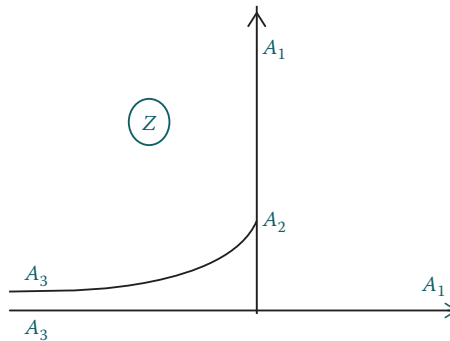


FIGURE 1.15 Physical flow plane.

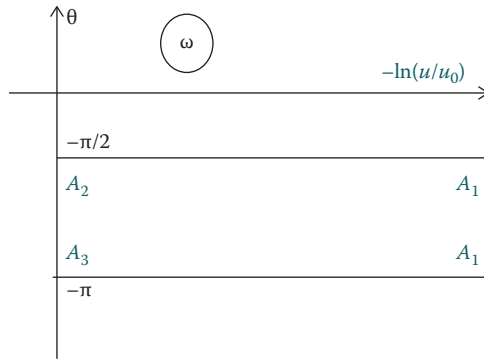


FIGURE 1.16 Plane of the Joukowski function.

On integrating, we obtain $\omega = C_1 \left(2 \ln(\sqrt{t+1} + \sqrt{t}) - i\pi \right) - \pi/2 \cdot i$. The constant C_1 is determined from the correspondence of the point A_3 . For $t = 0$, the function is $\omega = -i\pi$; therefore, $C_1 = 1/2$ and

$$\omega = \ln(\sqrt{t+1} + \sqrt{t}) - i\pi. \tag{1.34}$$

Using Equation 1.31, we will find a connection between the physical plane z and the parametric one t :

$$z = \frac{1}{u_0} C_1 \int_{-1}^t e^{\ln(\sqrt{t+1} + \sqrt{t}) - i\pi} \frac{dw}{dt} dt + C_2. \tag{1.35}$$

Since a point sink is in the plane t at A_3 , then the complex velocity is $\frac{dw}{dt} = -\frac{Q}{\pi t} = -\frac{u_0 \delta}{\pi t}$, so, after simple transformations of Equation 1.35 we obtain

$$z = C_1 \frac{\delta}{\pi} \int_{-1}^t \left(\frac{\sqrt{t+1}}{t} + \frac{1}{\sqrt{t}} \right) dt + C_2, \tag{1.36}$$

where $C_2 = iB$, as with $t = -1 \Rightarrow z = iB$.

On integrating, we obtain

$$z = C_1 \frac{\delta}{\pi} \left[2(\sqrt{t+1} + \sqrt{t}) + \ln \frac{\sqrt{t+1} - 1}{\sqrt{t+1} + 1} - i(\pi + 2) \right] + iB. \tag{1.37}$$

The constant C_1 is determined from the correspondence of the point A_3 in the planes t and z . For $t = \varepsilon \rightarrow 0$, the function is $z = -\infty$ (Figures 1.15 and 1.17). Then, substituting in Equation 1.37 we obtain

$$-\infty = C_1 \frac{\delta}{\pi} [2 - \infty - i(\pi + 2)] + iB. \tag{1.38}$$

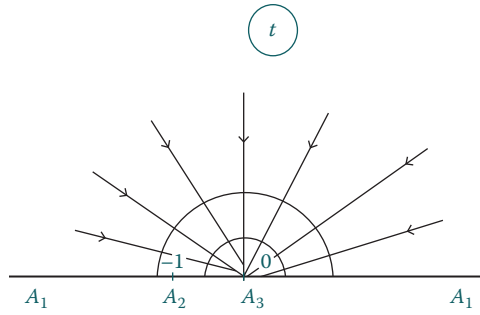


FIGURE 1.17 Parametric plane.

We equate the imaginary parts and find $C_1 = \frac{B\pi}{(\pi + 2)\delta}$. We have to now determine the half-width of the jet at infinity δ . For $t = -\varepsilon \rightarrow 0$ the function is $z = -\infty + i\delta$ (Figures 1.15 and 1.17). From Equation 1.37, we obtain

$$-\infty + i\delta = C_1 \frac{\delta}{\pi} [2 - \infty + i\pi - i(\pi + 2)] + iB. \tag{1.39}$$

From the equality of the imaginary parts, find $\delta = B\pi/(\pi + 2C_1)$ using the expression for C_1 , then, finally define $C_1 = 1$, $\delta = B(\pi/\pi + 2)$, and substituting in Equation 1.37, we obtain

$$z = \frac{B}{\pi + 2} \left[2(\sqrt{t+1} + \sqrt{t}) + \ln \frac{\sqrt{t+1} - 1}{\sqrt{t+1} + 1} \right]. \tag{1.40}$$

The complex velocity in the plane z is

$$\frac{dw}{dz} = \frac{dw}{dt} \frac{dt}{dz} = -\frac{u_0}{(\sqrt{t+1} + \sqrt{t})}. \tag{1.41}$$

The algorithm to calculate the axial velocity at a slot-type suction built into a flat infinite wall consists of the following steps:

1. The initial coordinate $x = 0$ is preset.
2. The formula $x = \frac{B}{\pi + 2} \left[2(\sqrt{t+1} + \sqrt{t}) + \ln \left(\frac{\sqrt{t+1} - 1}{\sqrt{t+1} + 1} \right) \right]$ is used to determine the parameter t .
3. The formula $u_x = -\frac{u_0}{\sqrt{t+1} + \sqrt{t}}$ is used to calculate the axial velocity of the air at x .
4. Perform the step $x = x + \Delta x$ and return to Step 2 until the set point is reached.

If the air suction rate is set as $u_0 = 1$, the axial velocity will take the values shown in Table 1.3.

TABLE 1.3
Values of the Axial Velocity of Separated Air Inflow to a Slot-Type Suction Unit Built in a Flat Infinite Wall

x/B	0	0.5	1	1.5	2	2.5	3	3.5	4	4.5	5
u	0.65	0.45	0.31	0.23	0.18	0.15	0.13	0.11	0.1	0.09	0.08

1.2.2 CALCULATION OF THE AIRFLOW AT THE SLOT-TYPE SUCTION IN INFINITE SPACE

Assume that the air from infinite space flows into a suction slot with a width $2B$ (Figure 1.18). The width of the jet at infinity is 2δ . Define the velocity value on the axis OX .

Due to the symmetry of the flow area (Figure 1.18), we disregard its lower part (Figure 1.19).

On the ray A_1A_2 , the velocity varies from 0 to u_0 and the real part of the Joukowski function $\text{Re } \omega$ decreases from ∞ down to 0. The direction of the velocity does not change, the angle to the axis OX $\theta = 0$, and, respectively, $\text{Im } \omega = 0$. On the line A_2A_3 , the velocity equals u_0 and $\text{Re } \omega$ and the imaginary part of the Joukowski function $\text{Im } \omega$ varies from 0 to $-\pi$. On the line A_3A_1 , $\text{Re } \omega$ increases from 0 to ∞ and $\text{Im } \omega = -\pi$. Thus, the area of the Joukowski function is a semiband (Figure 1.20).

Map the area ω onto the parametric plane t (see Figure 1.17) using the Schwarz–Christoffel formula:

$$\omega = C_1 \int_0^t \frac{dt}{\sqrt{t}\sqrt{t+1}} + C_2. \tag{1.42}$$

The constant C_1 is determined from the correspondence $t = 0 \Rightarrow \omega = -i\pi \Rightarrow C_1 = -i\pi$. Integrate Equation 1.42 using $t = -1 \Rightarrow \omega = 0$, we define $C_1 = 1$. Thus,

$$\omega = 2 \ln(\sqrt{t} + \sqrt{t+1}) - i\pi. \tag{1.43}$$

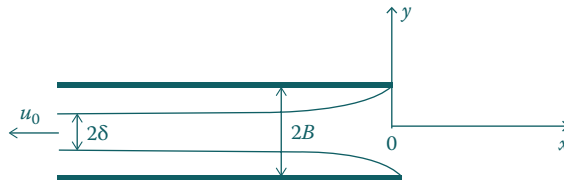


FIGURE 1.18 Jet separation at the freely spaced slot-type suction.

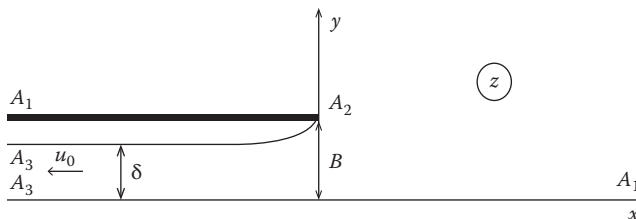


FIGURE 1.19 Physical flow plane.

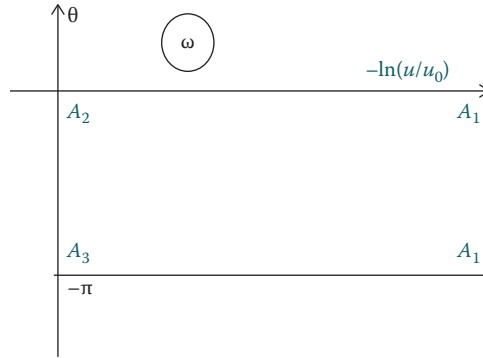


FIGURE 1.20 Area of the Joukowski function.

Using Equation 1.31, we find a connection between the physical flow plane and the parametric one:

$$z = C_1 \frac{\delta}{\pi} \int_{-1}^t \frac{(\sqrt{t} + \sqrt{t+1})^2}{t} dt + C_2, \quad (1.44)$$

where $C_1 = iB$, as for $t = -1 \Rightarrow z = iB$.

After integrating Equation 1.44 and using the correspondences $t = +\varepsilon \rightarrow 0 \Rightarrow z = -\infty$ and $t = -\varepsilon \rightarrow 0 \Rightarrow z = -\infty + i\delta$, we obtain $C_1 = 1$, $\delta = B/2$, so

$$z = \frac{B}{2\pi} \left[(\sqrt{t} + \sqrt{t+1})^2 + 1 + \ln t + 2 \ln(\sqrt{t} + \sqrt{t+1}) \right]. \quad (1.45)$$

The complex velocity is

$$\frac{dw}{dz} = -\frac{u_0}{(\sqrt{t} + \sqrt{t+1})^2}. \quad (1.46)$$

Then, the algorithm for calculating the axial velocity at a freely spaced slot-type suction unit consists of four steps:

1. The initial coordinate $x = 0$ is preset.
2. The formula $x = \frac{B}{2\pi} \left[(\sqrt{t} + \sqrt{t+1})^2 + 1 + \ln t + 2 \ln(\sqrt{t} + \sqrt{t+1}) \right]$ is used to determine the parameter t .
3. The formula $u_x = -\frac{u_0}{(\sqrt{t} + \sqrt{t+1})^2}$ is used to calculate the axial velocity of the air at x .
4. Perform the step $x = x + \Delta x$ and return to Step 2. Calculate until the predetermined point is reached.

The calculation results for $u_0 = 1$ (Tables 1.3 and 1.4) show that a suction unit built in a flat wall is more efficient just similar to the unseparated flow model.

TABLE 1.4
Values of the Axial Velocity of Separated Air Inflow to a Slot-Type Suction Unit in an Infinite Space

x/B	0	0.5	1	1.5	2	2.5	3	3.5	4	4.5	5
u	0.64	0.39	0.23	0.16	0.11	0.09	0.07	0.06	0.05	0.04	0.039

1.3 CALCULATION OF THE FLOW AT THE ENTRANCE OF THE SLOT-TYPE SUCTION BELL

This chapter presents some results of a study of a flow at a slot-type *long* suction bell, that is, having two successive vortex zones (Figure 1.21). A series of articles [124] contain detailed descriptions of the development of design ratios using the complex variable theory.

1.3.1 DESIGN RATIOS

The system of equations required for the calculation is as follows:

$$\beta = \frac{(n-h)(h-m)}{\sqrt{(h+1)(h-e)(h-d)h(1-h)}}, \quad K = \frac{\sqrt{2(1-e)(1-d)(1-h)}}{(1-n)(1-m)},$$

$$\beta = K \int_{-1}^e \frac{(t-n)(t-m)}{(t+1)(e-t)(d-t)|t|} \frac{dt}{(t-h)(t-1)},$$

$$\ln \frac{v_1}{v_2} = -K \int_e^d \frac{(t-n)(t-m)}{(t+1)(t-e)(d-t)|t|} \frac{dt}{(t-h)(t-1)},$$

$$l = \frac{L}{\pi v_2} \int_0^h e^{-\operatorname{Re} \chi(t)} \frac{dt}{1-t^2},$$

$$\operatorname{Re} \chi(t) = K \int_0^\zeta \frac{(t-n)(t-m)}{\sqrt{(t+1)(t-e)(t-d)t}} \frac{dt}{(t-h)(t-1)} + \ln \frac{v_1}{v_2},$$

$$\frac{L}{\pi v_2} \operatorname{Im} \int_0^e \frac{e^{-\chi(t)}}{t^2-1} dt = -l \sin \beta, \quad \frac{L}{\pi v_2} \operatorname{Re} \int_0^e \frac{e^{-\chi(t)}}{t^2-1} dt = -l \cos \beta,$$

$$\frac{L}{2v_1} \left(\frac{1-h}{h} \right)^{-\beta \cos \beta} e^{-\chi_1(1)} \left(\frac{1}{2} + \frac{\beta}{\pi} \frac{1}{1-h} + \chi_1(1) \right),$$

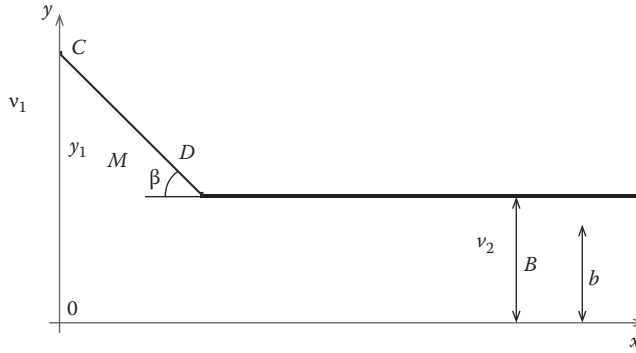


FIGURE 1.21 Slot-type suction bell with two vortex zones.

where

h, d, m, n, e are the parameters of mapping

$$\chi_1(1) = \int_0^1 \left[Kf(t) + \frac{\beta}{\pi f(h)} \frac{f(t) - f(h)}{t - h} + \frac{1}{f(1)} \frac{f(t) - f(1)}{t - 1} \right] dt$$

$$\chi'_1(1) = Kf'(1) + \frac{\beta}{\pi f(h)} \frac{f(1) - f(h)}{1 - h} + \frac{f'(1)}{f(1)}$$

$$f(t) = \frac{1}{\sqrt{t(t-e)(t-d)(t+1)}}$$

$$f'(1) = -\frac{1}{2} \frac{2(1-d)(2-e) + (1-e)(3-d)}{[2(1-e)(1-d)]^{3/2}}$$

This system of equations can be reduced to the solution of two equations for two unknowns e, d :

$$\begin{cases} f_1(e, d) = \sin \beta - (\text{int } 1 \cdot \sin \beta + \text{int } 2) / \text{int } 3 = 0, \\ f_2(e, d) = \cos \beta - (\text{int } 1 \cdot \cos \beta + \text{int } 4) / \text{int } 3 = 0, \end{cases} \quad (1.47)$$

where

$$\text{int } 1 = \int_e^d \exp \left[K \int_e^t f(\tau) d\tau \right] \frac{dt}{1-t^2}$$

$$\text{int } 2 = \exp(S_2) \cdot \int_d^0 \sin \left(\beta - K \cdot \int_d^t f(\tau) d\tau \right) \frac{dt}{1-t^2}$$

$$S_2 = K \int_e^d f(t) dt$$

$$\text{int } 3 = \exp(S_2) \int_0^h \exp \left[-K \int_0^t f(\tau) d\tau \right] \frac{dt}{1-t^2}.$$

$$\text{int } 4 = \exp(S_2) \cdot \int_d^0 \cos \left(\beta - K \cdot \int_d^t f(\tau) d\tau \right) \frac{dt}{1-t^2}$$

$$K = \frac{\beta + B_1 \int_{-1}^e \frac{dt}{(t-h)(t-1)r(t)} - A_1 \int_{-1}^e \frac{tdt}{(t-h)(t-1)r(t)}}{\int_{-1}^e \frac{dt}{r(t)}} \quad (1.48)$$

$$m = \frac{A}{2} - \sqrt{\frac{A^2}{4} + B}$$

$$n = \frac{A}{2} + \sqrt{\frac{A^2}{4} + B}$$

$$r(t) = \sqrt{|t(t+1)(t-e)(t-d)|}$$

$$f(t) = \frac{(t-n)(t-m)}{(t-h)(t-1)r(t)}$$

$$A = 1 + h - \frac{A_1}{K}$$

$$B = \frac{B_1}{K} - h$$

$$B_1 = \frac{\beta}{\pi} r(h) + h \cdot r(1)$$

$$A_1 = \frac{\beta}{\pi} r(h) + r(1)$$

The integrals in Equation 1.47 generally have singularities of the order $(x-a)^{1/2}$ (i.e., the denominator of the integrand goes to zero for $x=a$), and, thus, they are convergent improper integrals.

Integrals of the type $\int_a^b \frac{f(y)}{\sqrt{b-y}} dy$, $\int_a^b \frac{f(y)}{\sqrt{(y-a)(b-y)}} dy$ are calculated using the Lobatto quadrature formulas [123]:

$$\int_a^b \frac{f(y)}{\sqrt{b-y}} dy = \sqrt{b-a} \sum_{i=1}^{n/2} 2A_i f(y_i), \quad (1.49)$$

where

$y_i = a + (b-a)(1-x_i^2)$, x_i are the nodes of the Gauss quadrature (positive terms)

n is their number (even-numbered)

A_i is the weighting factors (corresponding to positive nodes x_i)

$$\int_a^b \frac{f(y)dy}{\sqrt{(y-a)(b-y)}} = \frac{\pi}{n} \sum_{i=1}^n f\left(\frac{b+a}{2} + \frac{b-a}{2} \cdot \cos \frac{(2i-1)\pi}{2n}\right). \quad (1.50)$$

Integrals without singularities were calculated using the Gauss quadratures

$$\int_a^b f(y)dy = \frac{b-a}{2} \sum_{i=1}^n A_i f(y_i), \quad (1.51)$$

where

$y_i = (a + b)/2 + (b-a)/2 \cdot x_i$, x_i are the nodes of the Gauss quadrature

n is their number

A_i are the weighting factors

In our calculations, the number of nodes n is 96 in the quadrature formulas of Equations 1.49 and 1.51 (and the interval of integration was sometimes divided into 10–500 parts to improve the accuracy of calculations) and is 40 in quadrature formula of Equation 1.50.

The parameter K is calculated by the formula

$$K = \frac{\beta + B_1 \cdot S_1 - A_1 \cdot S_2}{S_3}, \quad (1.52)$$

where the integrals S_1, S_2, S_3 are defined as follows:

$$S_1 = \int_{-1}^e \frac{dt}{(t-h)(t-1)\sqrt{t(t+1)(t-e)(t-d)}}$$

$$= \int_{-1}^e \frac{1}{(t-h)(t-1)\sqrt{(t(t-d)(e-t)(t+1))}} \frac{dt}{\sqrt{(e-t)(t+1)}} = \frac{\pi}{n} \sum_{i=1}^n \frac{1}{(t_i-h)(t_i-1)\sqrt{t_i(t_i-d)}},$$

where

$$t_i = \frac{e-1}{2} + \frac{e+1}{2} \cos \frac{(2i-1)\pi}{2n}$$

$$S_2 = \int_{-1}^e \frac{tdt}{(t-h)(t-1)\sqrt{|t(t+1)(t-e)(t-d)|}} = \frac{\pi}{n} \sum_{i=1}^n \frac{t_i}{(t_i-h)(t_i-1)\sqrt{|t_i(t_i-d)|}}$$

$$S_3 = \int_{-1}^e \frac{dt}{\sqrt{|t(t+1)(t-e)(t-d)|}} = \frac{\pi}{n} \sum_{i=1}^n \frac{1}{\sqrt{|t_i(t_i-d)|}}$$

Consider the calculation of the integrals in Equation 1.47.

The inner integral is

$$\int_e^t f(\tau)d\tau = \int_e^t \frac{(\tau-n)(\tau-m)d\tau}{(\tau-h)(\tau-1)\sqrt{|\tau(\tau+1)(\tau-e)(\tau-d)|}} = \{\text{particularity, if } \tau = e\}$$

$$= \int_e^t \frac{g(\tau)}{\sqrt{\tau-e}} d\tau = \int_{2e-t}^e \frac{g(2e-\tau)}{\sqrt{e-\tau}} d\tau = \sqrt{t-e} \sum_{j=1}^{n/2} 2A_j g(2e-\tau_j),$$

where $\tau_j = (2e-t) + (t-e)(1-x_j^2)$.

The outer integral is

$$\text{int 1} = \frac{d-e}{2} \sum_{i=1}^n A_i \frac{\exp \left[K \sqrt{t_i - e} \sum_{j=1}^{n/2} 2A_j g(2e - \tau_j) \right]}{1 - t_i^2},$$

where

$$t_i = \frac{d+e}{2} + \frac{d-e}{2} x_i$$

$$\tau_j = (2e - t_i) + (t_i - e)(1 - x_j^2)$$

$$S_2 = K \int_e^d \frac{(t-n)(t-m)dt}{(t-h)(t-1)\sqrt{|t(t+1)|}\sqrt{(t-e)(d-t)}} = \frac{\pi}{n} K \sum_{i=1}^n \frac{(t_i-n)(t_i-m)}{(t_i-h)(t_i-1)\sqrt{|t_i(t_i+1)|}}$$

$$t_i = \frac{d+e}{2} + \frac{d-e}{2} \cos \frac{(2i-1)\pi}{2n}$$

The integral is

$$\text{int 2} = \exp(S_2) \cdot \int_d^0 \sin \left(\beta - K \cdot \int_d^t f(\tau) d\tau \right) \frac{dt}{1-t^2}.$$

The inner integral is

$$\int_d^t f(\tau) d\tau = \{\text{see Section 1.3.1}\} = \sqrt{t-d} \sum_{j=1}^{n/2} 2A_j g(2d - \tau_j),$$

where $\tau_j = (2d - t) + (t - d)(1 - x_j^2)$.

The outer integral is

$$\text{int 2} = \exp(S_2) \cdot \frac{(-d)}{2} \sum_{i=1}^n \frac{A_i}{1-t_i^2} \cdot \sin \left(\beta - K \sqrt{t_i - d} \sum_{j=1}^{n/2} 2A_j g(2d - \tau_j) \right),$$

where

$$t_i = \frac{d}{2}(1 - x_i)$$

$$\tau_j = (2d - t_i) + (t_i - d)(1 - x_j^2)$$

The integral int 4 is calculated in the same way.

The integral is

$$\text{int 3} = \exp(S_2) \int_0^h \exp \left[-K \int_0^t f(\tau) d\tau \right] \frac{dt}{1-t^2}.$$

The inner integral has a singularity for $\tau = 0$ and is calculated as follows:

$$\int_0^t f(\tau) d\tau = \int_0^t \frac{(\tau - n)(\tau - m) d\tau}{(\tau - h)(\tau - 1) \sqrt{|\tau(\tau + 1)(\tau - e)(\tau - d)|}} = \int_0^t \frac{g(\tau)}{\sqrt{\tau}} d\tau = \int_{-t}^0 \frac{g(-\tau)}{\sqrt{0 - \tau}} d\tau = \sqrt{t} \sum_{j=1}^{n/2} 2A_j g(-\tau_j),$$

where $\tau_j = -t \cdot x_j^2$.

The required integral is determined by the formula

$$\text{int 3} = \exp(S_2) \cdot \frac{h}{2} \sum_{i=1}^n \frac{A_i}{1 - t_i^2} \cdot \exp\left(-K \sqrt{t_i} \sum_{j=1}^{n/2} 2A_j g(-\tau_j)\right),$$

where

$$t_i = \frac{h(x_i + 1)}{2}$$

$$\tau_j = -t_i \cdot x_j^2$$

System of Equation 1.47 is nonlinear and can be solved using the half-interval method.

For ease of computation, we write the system of equations to be solved as follows:

$$\begin{cases} f_1(e, d) - f_2(e, d) = 0, \\ f_2(e, d) = 0. \end{cases}$$

The algorithm for determining the roots is as follows:

1. Assign the interval at which we find the root of e : $[niz_e, ver_e]$.
2. Calculate the mean $e_c = (niz_e + ver_e)/2$.
3. Separate the interval $[niz, ver]$ at which the root d of $f_1(niz_e, d) - f_2(niz_e, d) = 0$ is located: To this end, make a loop on d and perform it until it satisfies the inequality

$$[f_1(niz_e, d) - f_2(niz_e, d)] \cdot f_1(niz_e, d + \Delta d) - f_2(niz_e, d + \Delta d) < 0.$$

Then, $niz = d$, $ver = d + \Delta d$, if d becomes positive (otherwise, there are no roots as the problem provides that $d > 0$).

4. Revision of the value d , for which $f_1(niz_e, d) - f_2(niz_e, d) = 0$. To do this, make a loop that is executed as long as $|f_1(niz_e, d) - f_2(niz_e, d)| > \varepsilon$ (ε is the set accuracy). Calculate $d = (niz + ver)/2$. Let us denote $d_1 = f_1(e, niz)$, $d_2 = f_2(e, niz)$, $d_3 = f_1(e, d)$, $d_4 = f_2(e, d)$. If $(d_1 - d_2)(d_3 - d_4) < 0$, then equate $ver = d$, otherwise $niz = d$.
5. Calculate the value $e_1 = f_2(niz_e, d)$.
6. Take the root of d , for which $f_1(e_c, d) - f_2(e_c, d) = 0$. Perform this as in Steps 3 and 4, where niz_e is used instead e_c .
7. If $e_1 \cdot f_2(e_c, d) < 0$, then $ver_e = e_c$, otherwise $niz_e = e_c$ and go to Step 2. This iterative process is terminated when the inequality $|niz_e - ver_e| < \varepsilon$ is achieved.

If at the first iteration $e_1 \cdot f_2(e_c, d) > 0$, then there are no roots and computing will end.

In our calculations, the computational error $\varepsilon = 0.00001$.

Calculate the velocity on the flow axis.

For this, we first calculate the parameter x_0 required to calculate the velocity,

$$\begin{aligned} x_0 &= -\frac{2}{\pi v_1} \int_0^{\infty} \exp\{K \cdot G_1(t)\} \cdot \sin[\pi + \beta + K \cdot G_2(t)] \frac{dt}{1+t^2} \\ &= \left\{ t = -\frac{x-1}{x}, \quad x = \frac{1}{1+t}, \quad dt = -\frac{dx}{x^2} \right\} \\ &= -\frac{2}{\pi v_1} \int_0^1 \exp\left\{K \cdot G_1\left(\frac{1-x}{x}\right)\right\} \cdot \sin\left[\pi + \beta + K \cdot G_2\left(\frac{1-x}{x}\right)\right] \frac{dt}{x^2 + (x-1)^2}, \end{aligned}$$

where

$$G_1\left(\frac{1-x}{x}\right) = \int_0^{(1-x)x} \frac{L_1(\tau)}{\sqrt{\tau}} \sin L_2(\tau) d\tau = \left\{ t = -\tau, \quad d\tau = -dt \right\} = \int_{(x-1)x}^0 \frac{L_1(t)}{\sqrt{0-t}} \sin L_2(t) dt.$$

The last integral is calculated using quadrature formula of Equation 1.49. The following denotations are introduced here:

$$\begin{aligned} L_1(t) &= \sqrt{\frac{(t^2 + m^2)(t^2 + n^2)}{(t^2 + h^2)(t^2 + 1)\sqrt{(t^2 + e^2)(t^2 + d^2)(t^2 + 1)}}}, \\ L_2(t) &= \left[\arccos \frac{-n}{\sqrt{t^2 + n^2}} + \arccos \frac{-m}{\sqrt{t^2 + m^2}} - \arccos \frac{-h}{\sqrt{t^2 + h^2}} - \arccos \frac{-1}{\sqrt{t^2 + 1}} \right] \\ &\quad - \frac{1}{2} \left[\frac{\pi}{2} + \arccos \frac{-d}{\sqrt{t^2 + d^2}} + \arccos \frac{-e}{\sqrt{t^2 + e^2}} + \arccos \frac{1}{\sqrt{t^2 + 1}} \right]. \end{aligned}$$

Introduce the denotations

$$\begin{aligned} P_1(\xi) &= \exp\left(-K \int_{-1}^{-\infty} f(t) dt + K \int_{\xi}^{\infty} f(t) dt\right), \quad 1 < \xi < \infty, \\ P_2(\xi) &= \exp\left(-K \int_{-1}^{-\infty} f(t) dt - K \int_{-\infty}^{\xi} f(t) dt\right), \quad -\infty < \xi < -1. \end{aligned}$$

We show that $P_1(\xi)$ and $P_2(\xi)$ are equal. Actually, the integrals

$$\int_{\xi}^{\infty} f(t) dt = \left\{ \tau = \frac{1}{t}, dt = -\frac{d\tau}{\tau^2} \right\} = -\int_{1/\xi}^0 f\left(\frac{1}{\tau}\right) \frac{d\tau}{\tau^2},$$

$$\int_{-\infty}^{\xi} f(t) dt = \left\{ \tau = \frac{1}{t}, dt = -\frac{d\tau}{\tau^2} \right\} = \int_{1/\xi}^0 f\left(\frac{1}{\tau}\right) \frac{d\tau}{\tau^2}.$$

Thus,

$$\int_{\xi}^{\infty} f(t) dt = -\int_{-\infty}^{\xi} f(t) dt.$$

It follows $P_1(\xi) = P_2(\xi) = P(\xi)$.

In the same manner, we can show that

$$\int_{\xi}^{\infty} P(t) \frac{dt}{t^2 - 1} = -\int_{-\infty}^{\xi} P(t) \frac{dt}{t^2 - 1}.$$

Thus, the required correspondence of the points for $|\xi| > 1$ will be determined by the relation

$$x(\xi) = x_0 - \frac{2}{\pi v_2} \int_{\xi}^{\infty} P(\tau) \frac{d\tau}{\tau^2 - 1},$$

where the integral can be represented for computational convenience as

$$\int_{\xi}^{\infty} P(\tau) d\tau = \left\{ \tau = \frac{1}{t} \right\} = \int_0^{\frac{1}{\xi}} P\left(\frac{1}{t}\right) \frac{dt}{1-t^2}.$$

The integrand is

$$P\left(\frac{1}{t}\right) = \exp(-K \cdot S_1) \cdot \exp\left(K \cdot \int_{1/t}^{\infty} f(\tau) d\tau\right), \quad S_1 = \int_{-1}^{-\infty} f(t) dt.$$

To avoid infinitely large limits of integration, transform the integrals as follows:

$$\int_{1/t}^{\infty} f(\tau) d\tau = \int_0^t f\left(\frac{1}{\tau}\right) \frac{d\tau}{\tau^2} = \int_0^t \frac{(1-\tau n)(1-\tau m) d\tau}{(1-h\tau)(1-\tau) \sqrt{(1+\tau)(1-\varepsilon\tau)(1-d\tau)}} = S_2(t).$$

Given the above, we finally obtain

$$x(\xi) = x_0 - \frac{2e^{-KS_1}}{\pi v_2} \int_0^{1/\xi} \exp(K \cdot S_2(t)) \frac{dt}{t^2 - 1} \quad \text{for } |\xi| > 1.$$

The velocity on the flow axis is calculated from the formula

$$v_x = \frac{v_2}{P(\xi)}, \quad |\xi| > 1,$$

where

$$P(\xi) = \exp[-K \cdot \{S_1 + S_2(\xi)\}], \quad S_2(\xi) = \int_{1/\xi}^0 f\left(\frac{1}{\tau}\right) \frac{d\tau}{\tau^2}.$$

Thus,

$$v_x = v_2 \cdot \exp[K \cdot \{S_1 + S_2(\xi)\}], \quad |\xi| > 1.$$

The positions of the points on the first free stream line (CMD) are determined from

$$x = -\frac{2}{\pi v_1} \int_0^{\xi} \frac{J_1(t) dt}{t^2 - 1}, \quad y = -\frac{2}{\pi v_1} \int_0^{\xi} \frac{J_2(t) dt}{t^2 - 1} + 1 + l \cdot \sin \beta.$$

The following denotations are introduced here:

$$J_1(t) = \cos \left[K \int_0^t f(\tau) d\tau - \beta \right], \quad J_2(t) = \sin \left[K \int_0^t f(\tau) d\tau - \beta \right].$$

The integrals were calculated using the Gauss quadratures.

1.3.2 CALCULATION RESULTS

Some results of the calculation that were not included in articles [124] are shown in Figures 1.22 through 1.33.

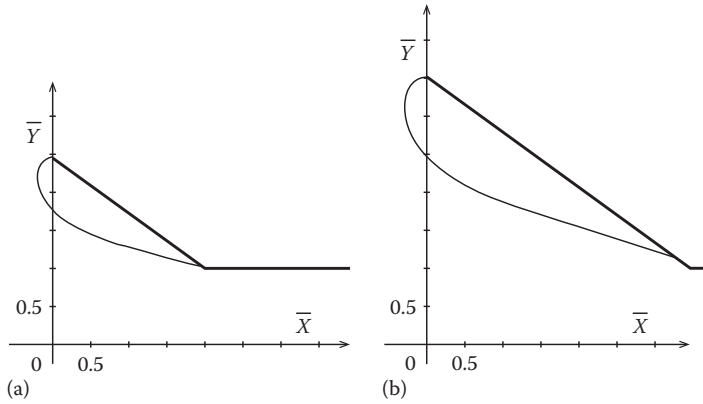


FIGURE 1.22 Form of the first free flow line for a bell expansion angle of 36: (a) $e = -0.99919$; $d = -0.99906$; $m = -0.9946$; $n = 0.462$; $h = 0.405$; $l = 2.474$; $v_1 = 0.818$; $v_2 = 1.209$; and (b) $e = -0.99985$; $d = -0.99935$; $m = -0.9941$; $n = 0.497$; $h = 0.44$; $l = 4.279$; $v_1 = 0.570$; $v_2 = 1.250$.

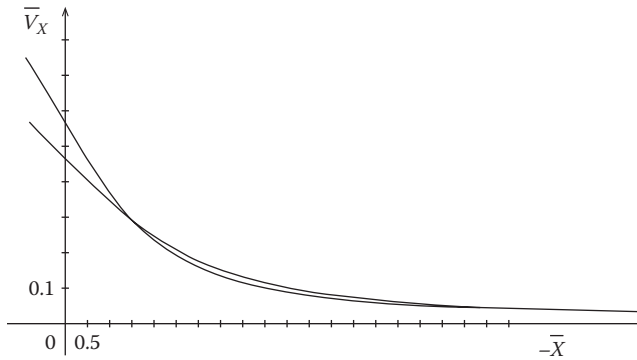


FIGURE 1.23 Change in the dimensionless axial velocity at a distance from the inlet for the cases (a) and (b) in Figure 1.22 (from top downward, respectively).

1.4 SIMULATION OF FLOW SEPARATION AT THE INLET OF A PROJECTING FLAT SUCTION CHANNEL

This chapter focuses on the numerical and experimental study of a separated flow at the inlet of a slot-type hooded suction inlet.

1.4.1 DETERMINATION OF DESIGN RATIOS

Assume that an infinitely wide horizontal pipe with a width $2B$ is projected to a distance S from the vertical wall. The pipe axis is directed along the axis OX of the physical plane of the complex variable $z = x + iy$. We will consider the upper part of the flow in the semiplane $y \geq 0$. We will use the upper semiplane of the complex variable $t = x_1 + iy_1$ as a parametric one. The correspondence of the points in these ranges, as well as the ranges of the unknown quantities of the Joukowski function $\omega = \ln(u_\infty/u) + i\theta$ and the complex potential function $w = \varphi + i\psi$, are shown in Figure 1.34. Here, u_∞ is the velocity value on the *free* flow line CD ; u is also in the arbitrary points of the area under review in the quadrilateral $ADCBA$ of the physical area $\text{Im}(z) \geq 0$.

The quadrilateral has two vertexes at infinity: the point A , at which a line source with a strength q is placed, and the point D , where a sink with the same strength is placed. Thus, the range of

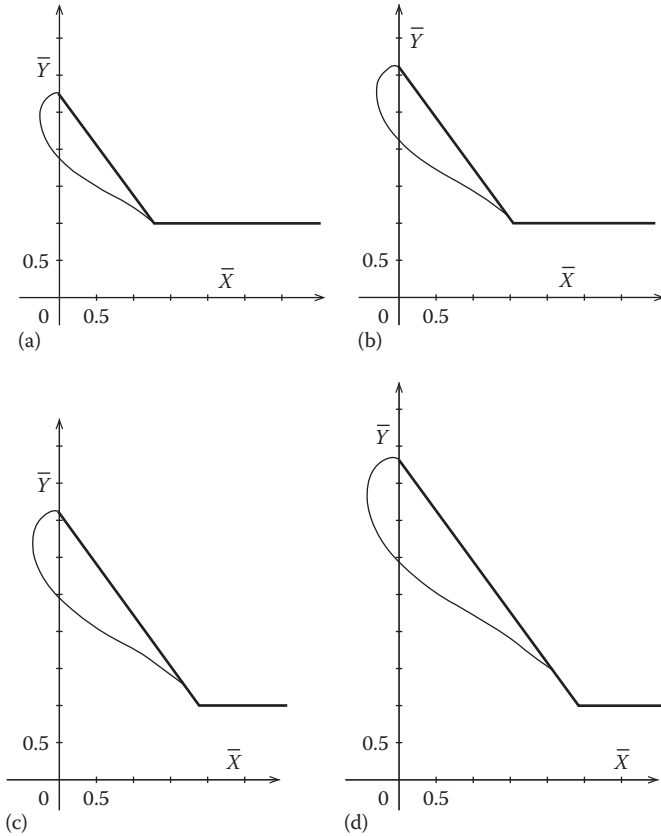


FIGURE 1.24 Form of the first free flow line for a bell expansion angle of 54°: (a) $e = -0.995$; $d = -0.993$; $m = -0.975$; $n = 0.382$; $h = 0.3$; $l = 2.143$; $v_1 = 0.704$; $v_2 = 1.341$; (b) $e = -0.997$; $d = -0.994$; $m = -0.975$; $n = 0.393$; $h = 0.31$; $l = 2.596$; $v_1 = 0.618$; $v_2 = 1.358$; (c) $e = -0.998$; $d = -0.994$; $m = -0.975$; $n = 0.403$; $h = 0.32$; $l = 3.214$; $v_1 = 0.531$; $v_2 = 1.371$; and (d) $e = -0.999$; $d = -0.995$; $m = -0.975$; $n = 0.413$; $h = 0.33$; $l = 4.108$; $v_1 = 0.442$; $v_2 = 1.378$.

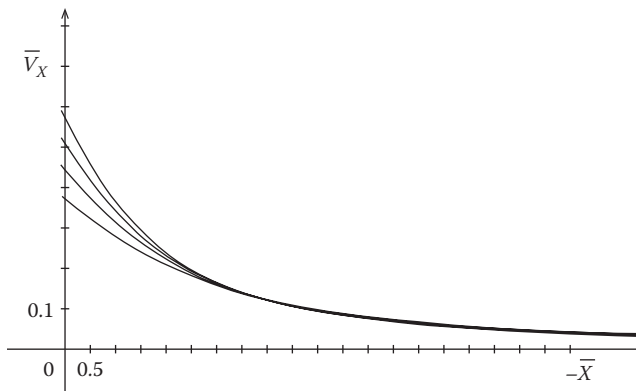


FIGURE 1.25 Change in the dimensionless axial velocity at a distance from the inlet for the cases (a), (b), (c), and (d) in Figure 1.24 (from top downward, respectively).

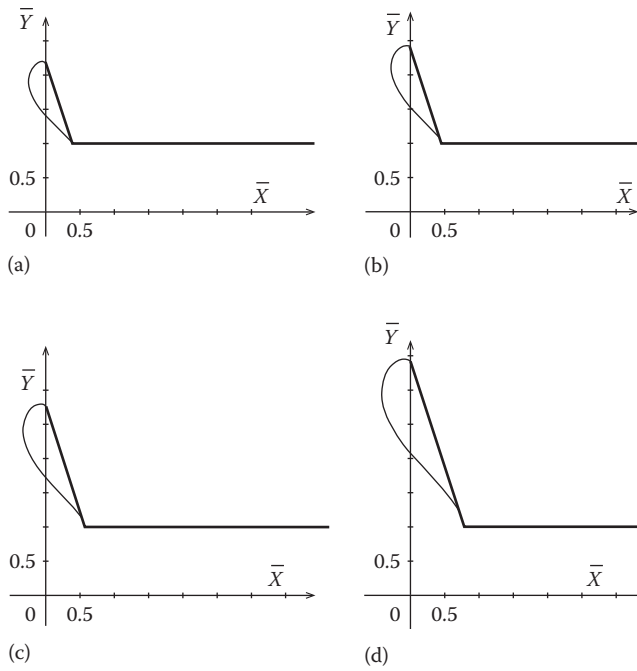


FIGURE 1.26 Form of the first free stream line with a bell expansion angle of 72° : (a) $e = -0.97$; $d = -0.968$; $m = -0.936$; $n = 0.301$; $h = 0.202$; $l = 1.235$; $v_1 = 0.835$; $v_2 = 1.435$; (b) $e = -0.975$; $d = -0.971$; $m = -0.936$; $n = 0.310$; $h = 0.21$; $l = 1.470$; $v_1 = 0.747$; $v_2 = 1.446$; (c) $e = -0.983$; $d = -0.975$; $m = -0.938$; $n = 0.321$; $h = 0.22$; $l = 1.854$; $v_1 = 0.64$; $v_2 = 1.461$; and (d) $e = -0.990$; $d = -0.979$; $m = -0.939$; $n = 0.334$; $h = 0.232$; $l = 2.533$; $v_1 = 0.513$; $v_2 = 1.476$.

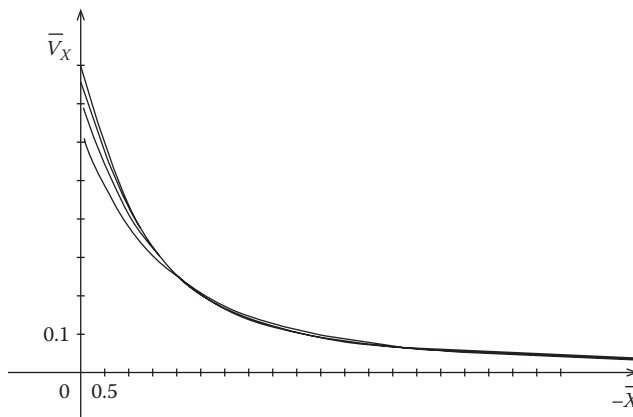


FIGURE 1.27 Change in the dimensionless axial velocity at a distance from the inlet for the cases (a), (b), (c), and (d) in Figure 1.26 (from top downward, respectively).

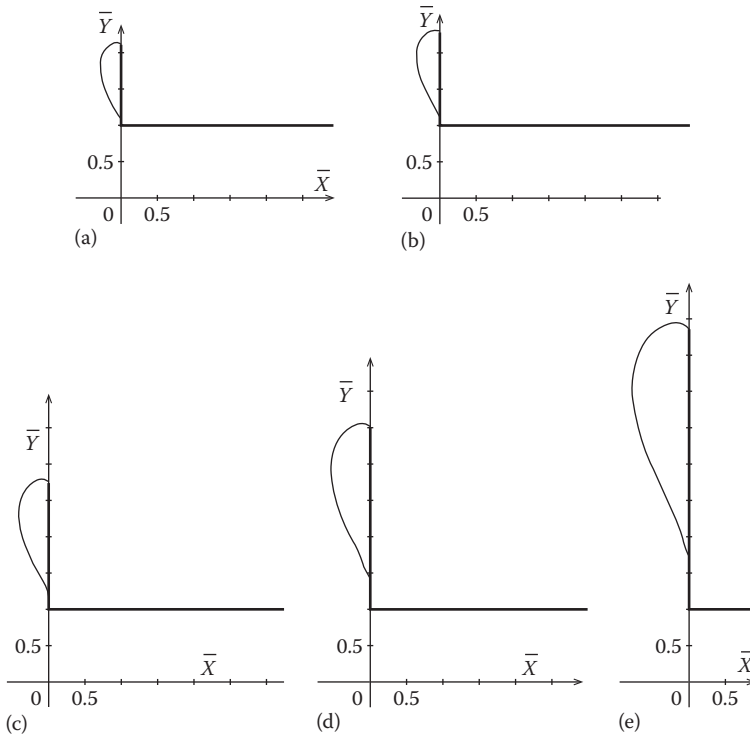


FIGURE 1.28 Form of the first free flow line for a bell expansion angle of 90° : (a) $e = -0.934$; $d = -0.926$; $m = -0.871$; $n = 0.255$; $h = 0.145$; $l = 1.096$; $v_1 = 0.771$; $v_2 = 1.546$; (b) $e = -0.944$; $d = -0.932$; $m = -0.874$; $n = 0.261$; $h = 0.15$; $l = 1.27$; $v_1 = 0.700$; $v_2 = 1.554$; (c) $e = -0.962$; $d = -0.942$; $m = -0.880$; $n = 0.274$; $h = 0.16$; $l = 1.738$; $v_1 = 0.564$; $v_2 = 1.564$; (d) $e = -0.976$; $d = -0.949$; $m = -0.856$; $n = 0.286$; $h = 0.17$; $l = 2.483$; $v_1 = 0.434$; $v_2 = 1.563$; and (e) $e = -0.988$; $d = -0.954$; $m = -0.890$; $n = 0.298$; $h = 0.18$; $l = 3.843$; $v_1 = 0.307$; $v_2 = 1.548$.

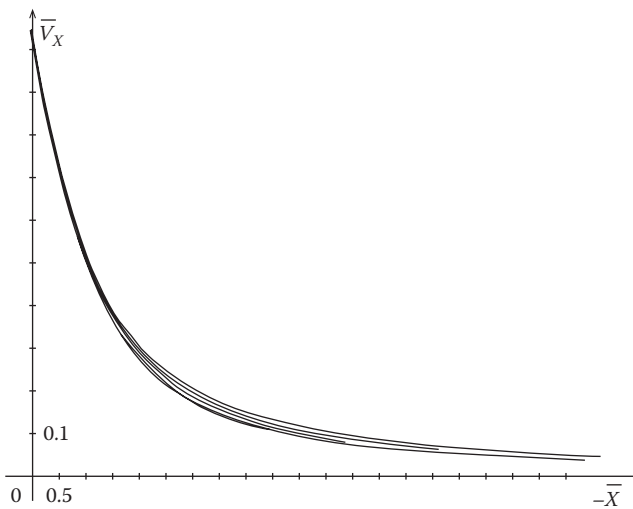


FIGURE 1.29 Change in the dimensionless axial velocity at a distance from the inlet for the cases (a), (b), (c), (d), and (e) in Figure 1.28 (from top downward, respectively).

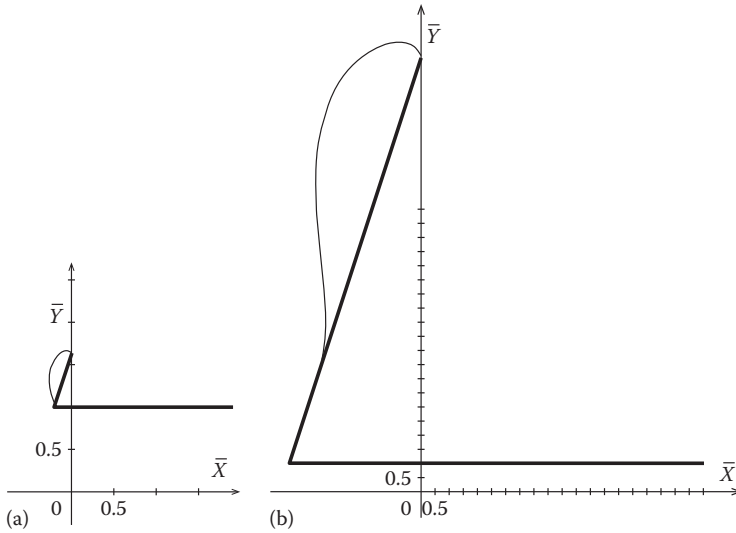


FIGURE 1.30 Form of the first free flow line with a bell expansion angle of 108° : (a) $e = -0.834$; $d = -0.828$; $m = -0.763$; $n = 0.200$; $h = 0.090$; $l = 0.66$; $v_1 = 0.917$; $v_2 = 1.636$; and (b) $e = -0.995$; $d = -0.919$; $m = -0.829$; $n = 0.271$; $h = 0.14$; $l = 15.079$; $v_1 = 0.075$; $v_2 = 1.209$.

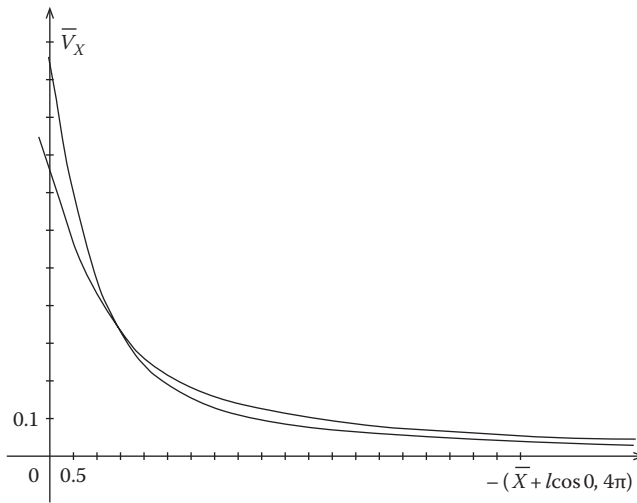


FIGURE 1.31 Change in the dimensionless axial velocity at a distance from the inlet for the cases (a) and (b) in Figure 1.30 (the upper and lower line, respectively).

the complex potential is a band bounded by the flow lines $\psi = 0$, $\psi = q$, and equipotential lines at infinity $\phi = \pm\infty$, and the range of the Joukowski function is a half-band with a cut along the ray $MA(\theta = -\pi/2)$ bounded by horizontal lines $\theta = 0$ and $\theta = -\pi$ (θ is the angle between the positive axis OX and the direction of the velocity vector \vec{u}).

Find a conformal mapping of the upper semiplane $\text{Im}(t) > 0$ onto the interior of the range ω (the interior of the pentagon $ADCBMA$ with two vertexes at infinity).

We use the Schwarz–Christoffel integral, after simple transformations, taking into account the transition conditions of the singular points B and B on semicircles $t = b + \varepsilon_b e^{i\alpha}$ and $t = 1 + \varepsilon_a e^{i\alpha}$

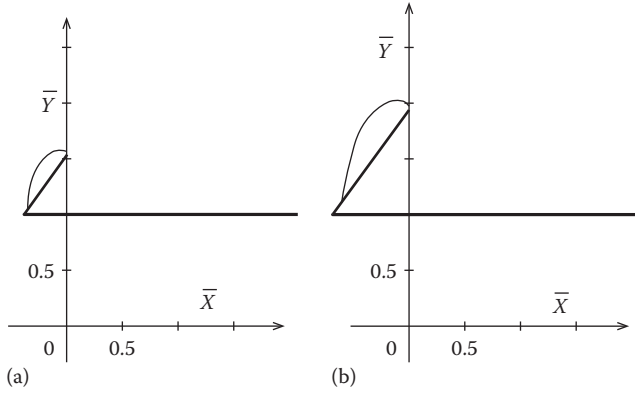


FIGURE 1.32 Form of the first free flow line for a bell expansion angle of 126°: (a) $e = -0.760$; $d = -0.739$; $m = -0.653$; $n = 0.171$; $h = 0.06$; $l = 0.653$; $v_1 = 0.790$; $v_2 = 1.714$; and (b) $e = -0.843$; $d = -0.790$; $m = -0.689$; $n = 0.189$; $h = 0.07$; $l = 1.174$; $v_1 = 0.534$; $v_2 = 1.674$.

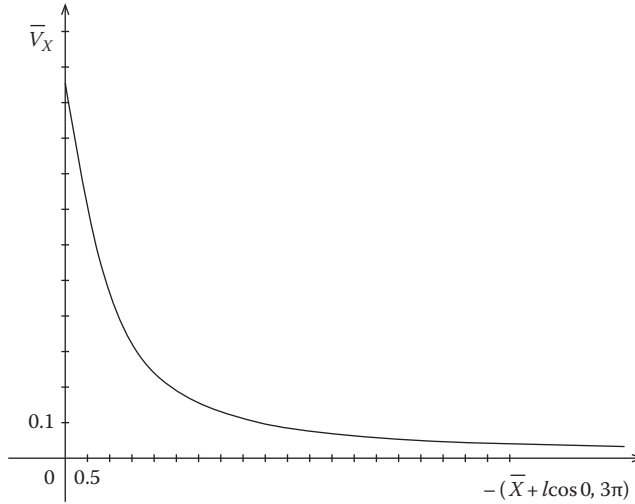


FIGURE 1.33 Change in the dimensionless axial velocity at a distance from the inlet for the case (b) in Figure 1.32.

($\epsilon_b \rightarrow 0$, $\epsilon_a \rightarrow 0$, $\alpha = \pi \dots 0$), as well as taking into account the correspondence of the points C and M , we find the desired Joukowski function

$$\omega = \frac{1}{2} \ln \left(\frac{\sqrt{t} + \sqrt{b}}{\sqrt{t} - \sqrt{b}} \cdot \frac{\sqrt{t} + 1}{\sqrt{t} - 1} \right) = \ln \frac{\sqrt{t} + \sqrt{b}}{\sqrt{t} - b} \cdot \frac{\sqrt{t} + 1}{\sqrt{t} - 1} \tag{1.53}$$

and define the parameter

$$\mu = \ln \frac{1 + b^{1/4}}{1 - b^{1/4}}. \tag{1.54}$$